Natural Resources Canada | Ressources naturelles Canada

GEOLOGICAL SURVEY OF CANADA
OPEN FILE 9185

Critical mineral resource potential of tailings from the former Saint Lawrence columbium mine, Oka, Quebec

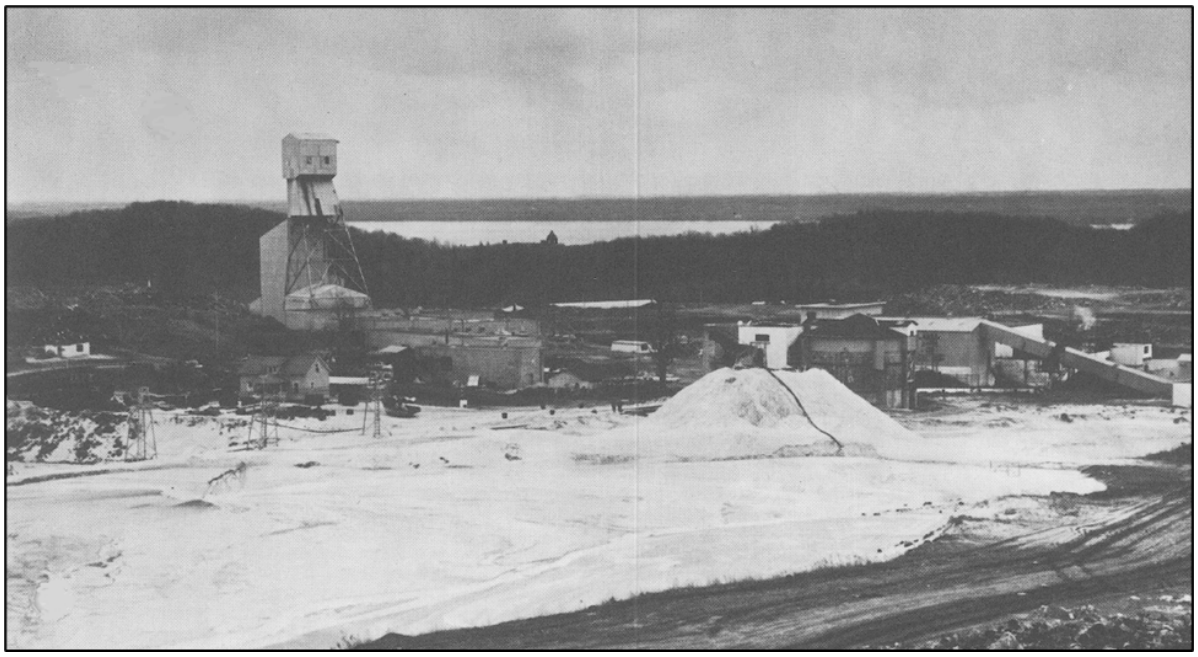

A.J. Desbarats, M. Beauchamp, I. Bilot, S. Madore, M.J. Polivchuk, M. Wygergangs, and J.B. Percival

2024

Canada

GEOLOGICAL SURVEY OF CANADA
OPEN FILE 9185

Critical mineral resource potential of tailings from the former Saint Lawrence columbium mine, Oka, Quebec

A.J. Desbarats, M. Beauchamp, I. Bilot, S. Madore, M.J. Polivchuk, M. Wygergangs, and J.B. Percival

2024

Permanent link: https://doi.org/10.4095/pwu5neguzc

This publication is available for free download through the NRCan Open Science and Technology Repository (https://ostrnrcan-dostrncan.canada.ca/).

Recommended citation

Desbarats, A.J., Beauchamp, M., Bilot, I., Madore, S., Polivchuk, M.J., Wygergangs, M., and Percival, J.B., 2024. Critical mineral resource potential of tailings from the former Saint Lawrence columbium mine, Oka, Quebec; Geological Survey of Canada, Open File 9185, 1 .zip file. https://doi.org/10.4095/pwu5neguzc

Publications in this series have not been edited; they are released as submitted by the author.

ISSN 2816-7155
ISBN 978-0-660-71953-5
Catalogue No. M183-2/9185E-PDF

FOREWORD

The Geological Survey of Canada's Critical Minerals Geoscience and Data (CMGD) program is focused on fourteen priority critical minerals, which are copper, nickel, zinc, rare earth elements (REE), cobalt, lithium, niobium, indium, germanium, scandium, tellurium, vanadium, tungsten, and graphite. These elements are investigated through all stages of their mining cycle, from exploration to extraction, with a view towards lowering the environmental, ecological, and social impacts of resource development. Objective #1 of the CMGD Program is to address knowledge gaps on the mineralogy and geochemistry of critical minerals. The proposed solution is to develop a critical minerals data base through a comprehensive sampling and analysis program to determine critical mineral contents of Canadian deposits and their associated products including ores, concentrates, waste rock, and tailings. This will provide freely-accessible mineralogical and geochemical information necessary to estimate critical mineral resources, inform potential value and supply options, and conduct robust economic modelling. This report is concerned with the niobium (Nb), phosphorus (P), and rare earth element (REE) contents of tailings from the past-producing Saint Lawrence Columbium (SLC) mine near Oka, Quebec. It describes the physical properties of the tailings, their mineralogy, and their bulk geochemistry. Results of this investigation illustrate the critical mineral resource potential of mine tailings and how environmental and social governance goals could be advanced by reprocessing material previously considered waste.

DISCLAIMER

Estimates of critical mineral resources presented in this report do not conform with recognized mineral resource reporting standards and were not intended to. They should not be relied upon as a basis for investment decisions.

Cover photograph: View of the Saint Lawrence Columbium mine site in 1967, looking south toward the Lake des Deux Montagnes. Photograph from SLC (1967).

SUMMARY

Between 1961 and 1976, the Saint Lawrence Columbium (SLC) mine produced pyrochlore concentrate and ferroniobium alloy from a carbonatite-hosted deposit near Oka, Quebec. Tailings generated by ore processing contain critical minerals including niobium (Nb), rare earth elements (REEs), and phosphorus (P). This report is concerned with characteristics of the tailings that could determine their critical mineral resource potential. It describes their physical properties, their mineralogy, and their bulk geochemistry. Measurements were made on split-spoon core samples obtained at continuous downhole intervals from a 25 m borehole penetrating the full thickness of the tailings impoundment.

Grain-size distribution data for the tailings show that they range in texture from medium sand to predominantly clayey silt. The average density, water content, and porosity of the tailings are 2.82 g/cm^3, 30%, and 47%, respectively. The mean plasticity index of the tailings is 11.3%. Based on historical mine production of about 5.7 million tonnes of ore, the 19.2 ha impoundment contains an estimated 3.8 million m^3 of tailings material with an average thickness of 20 m.

Bulk X-ray Diffraction (XRD) analyses show that the tailings are composed mainly of calcite (64-89 wt. %), biotite (6-17 wt.%), fluorapatite (2-22 wt.%), and chlorite (0-5 wt.%). Scanning Electron Microscopy (SEM) reveals that tailings also contain a considerable diversity of minor and trace gangue minerals including ferroan dolomite, nepheline, monticellite, richterite, pyrite, sphalerite, magnetite, perovskite, and pyrochlore. From a critical minerals perspective, the tailings are of interest for their unrecovered pyrochlore and apatite contents. Pyrochlore and apatite are the mineral hosts of Nb and P, respectively. However, Energy Dispersive Spectroscopy (EDS) and Electron Probe Microanalyses (EPMA) show that both pyrochlore and apatite are highly enriched in REE as well. Based on historical mine production figures and estimates of Nb recovery efficiency, the tailings contain 0.15 wt.% Nb_2O_5 or about 0.3wt.% pyrochlore. Based on XRD analyses of tailings samples conducted here, the average P_2O_5 and apatite contents of the tailings are 2.46 wt.% and 5 wt.%, respectively. Both pyrochlore and apatite exhibit similar REE enrichment distribution patterns dominated by light rare earth elements. Average total rare earth oxide (ΣREEO) in pyrochlore and apatite grains are in the ranges of 9.62 to 10.42 wt.% and 2.47 to 3.25 wt.%, respectively.

Historical air photographs show that tailings disposal practices for the different waste streams from the SLC mill varied over the life of the mine. This is manifested by significant tailings heterogeneity observed in the stratigraphic borehole. Notably, near the base of the impoundment, a thin 2 m layer of dense, coarse-grained material contains up to 0.76 wt.% Nb_2O_5 and 7.74 wt.% P_2O_5 (or about 22% apatite) as well as abundant magnetite and sulfide minerals. Other depth horizons are dominated by fine-textured tailings containing abundant biotite and chlorite, which adversely affected mill recovery during mining operations. These factors highlight the need for systematic drilling of historical tailings impoundments in order to assess their critical mineral resource potential with confidence.

TABLE OF CONTENTS

1. INTRODUCTION

1.1 Background

The emergence of new green technologies is driving increased demand for advanced materials containing metals and other elements termed "critical" due to their scarcity or risk of supply disruption. Natural Resources Canada (NRCan) has identified 31 elements that are critical for Canada's economic security and for its transition to a low carbon economy (Figure 1). As part of Canada's Critical Minerals Strategy, the Critical Minerals Geoscience and Data (CMGD) Program of the Geological Survey of Canada (GSC) is focused on 14 priority critical elements, namely copper, nickel, zinc, rare earth elements (REE), cobalt, lithium, niobium, indium, germanium, scandium, tellurium, vanadium, tungsten, and graphite. The objectives of this program are 1) to address knowledge and data gaps on the mineralogy and geochemistry of priority critical minerals; 2) to conduct thematic research on new sources of critical minerals, including mine waste, brines, and clays, with improved Environmental, Social and Governance (ESG) performance; and 3) to build predictive mineral intelligence to support the discovery of critical minerals. This report addresses the first objective by contributing to Canada's critical minerals knowledge base through systematic sampling and analysis of the critical mineral content of ore deposits and their derivative products such as mine wastes.

The depletion of easily accessible orebodies and societal concerns about the environmental impacts of new mining projects are prompting a reappraisal of mine wastes as potentially valuable mineral resources (Lottermoser, 2011; Seal and Piatak, 2017). Re-processing of mine wastes such as tailings offers the possibility of securing new mineral supplies while mitigating the environmental footprint of current and historical mining operations. This is particularly the case for critical minerals, which are often found in mine wastes as unrecovered by-products of the primary mineral commodity (Dold, 2020; Vitti and Arnold, 2022). However, the estimation and classification of critical mineral resources hosted in by-product wastes is a significant challenge (Mudd et al., 2017; Werner et al., 2017; Araya et al., 2021; Suppes and Heuss-Aßbichler, 2021). New approaches are being developed for assessing critical minerals resources hosted by tailings (Nikonow et al., 2019; Mulenshi et al., 2021; Blannin et al., 2023). These include compilation of information on ore deposit geology and on the mineral processing flow sheet as well as detailed characterization of the granulometry, geochemistry, and mineralogy of the tailings (NRCan, 2022).

Carbonatite intrusions are enriched in numerous incompatible elements including Nb, Ta, REEs, Zr, Ba, P, F, Mo, Sr, V, Th, and U. Because of this, they represent attractive targets for several critical metals although they are most often mined for Nb and REEs (Modereski et al., 1995; Richardson and Birkett, 1996; Woolley and Kjarsgaard, 2008; Berger et al., 2009; Weng et al., 2013; Mitchell, 2015; Simandl and Paradis, 2018). In Canada, several undeveloped carbonatite deposits are being considered as sources of Nb or REEs (or both) and one (Niobec) is currently (2024) being mined for Nb (Richardson and Birkett, 1996; Simandl and Paradis, 2018). However, the past-producing Saint Lawrence Columbium (SLC) mine near Oka, Quebec, is another carbonatite-hosted Nb-REE deposit where tailings stored on site represent a potential source of critical minerals. This report is concerned with the critical mineral content of these tailings, as well as their physical properties and geochemistry.

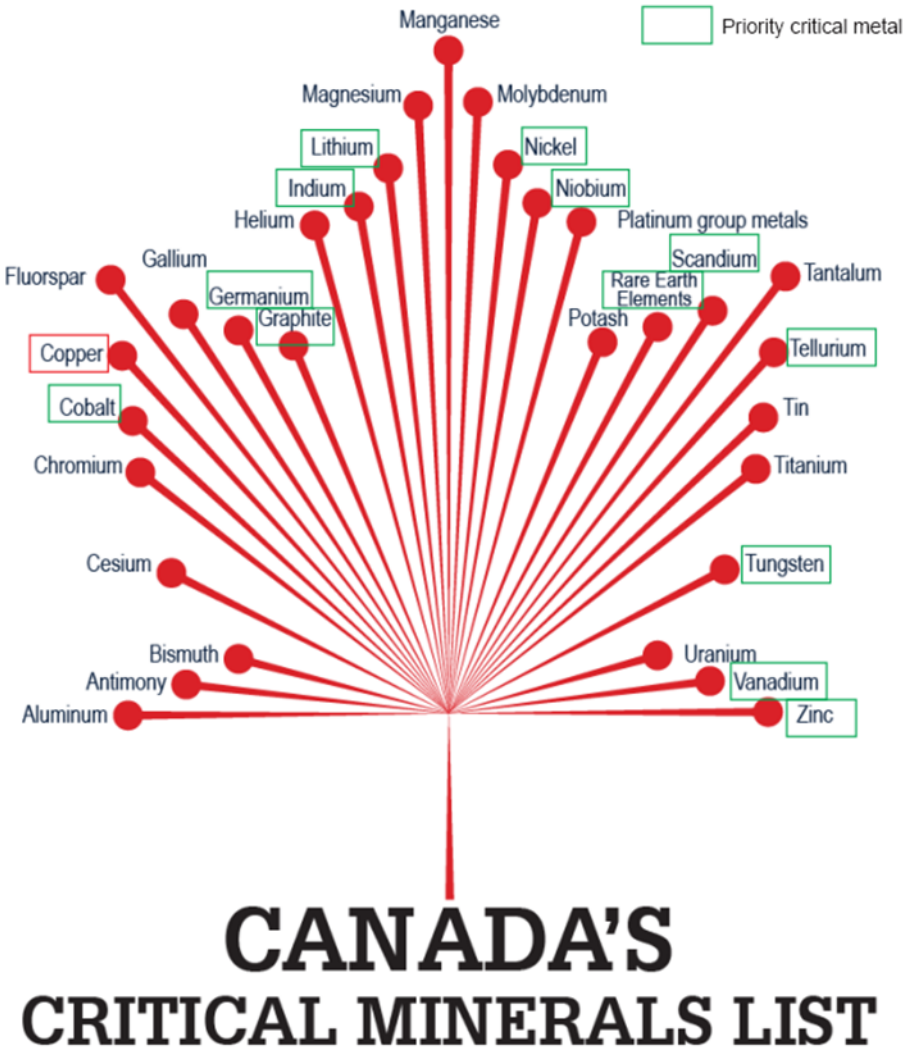

Figure 1: Canada's critical mineral list with priority critical minerals highlighted. (Natural Resources Canada; www.nrcan.gc.ca/criticalminerals)

1.2 The Saint Lawrence Columbium Mine

The discovery of radioactive minerals near Oka during the 1950s uranium exploration boom prompted the Saint Lawrence River Mining syndicate to stake a large portion of the surrounding area in early 1954. While the original exploration target was uranium, the greater economic significance of the niobium (columbium) content of the Oka carbonatite soon became apparent after drilling revealed the presence of several mineralized lenses and large bodies of low-grade pyrochlore-bearing rocks (Carbonneau and Caron, 1965). However, the challenge was to develop a viable pyrochlore concentration process. Research carried out at the École Polytechnique in Montréal, and the Department of Mines and Technical Surveys in Ottawa eventually led to the design and construction of a pilot plant in 1959. The plant was able to achieve a 50 % Nb_2O_5 concentrate from a head grade of 0.4 % Nb_2O_5. After the original mining syndicate merged with another company, the newly formed Saint Lawrence Columbium and Metals Corporation (SLC) started construction of a 500 tons/day mill on the site. Mining and concentrate production started in October of 1961. At that time, SLC's Oka mine was the world's first primary producer of Nb_2O_5 as well as the single largest producer (Carbonneau and Caron, 1965).

Initially, ore was obtained from two open pits. Underground mining started in 1965 with access to the workings from an adit in the wall of the deeper pit. Following the completion of a 410 m (1345 ft.) shaft in late 1966, production shifted completely underground in 1968. In 1971, the shaft was deepened to 586 m (1922 ft.) to access higher-grade reserves at depth. Throughout the mine life, mill capacity was gradually increased to 1700 tons/d in 1967, 2200 tons/d in 1972, and then 3000 tons/d in 1975. At the same time, modifications to the milling process improved pyrochlore recovery (Carbonneau and Caron, 1965; SLC, 1967). With research funding from the federal government, a new lower cost and higher efficiency concentrator flowsheet was developed, and plans were made to reprocess mine tailings containing an estimated 12 million pounds of Nb_2O_5 (SLC, 1971). Starting in 1972, the original milling process was phased out in favour of the new process, which was implemented in a parallel milling circuit (SLC, 1972). Meanwhile, in 1969, the company constructed a small-scale plant for custom production of ferroniobium alloy (FeNb), the form of niobium required by most end users (SLC, 1969). To meet increasing demand from the steel industry, the company began building a new full-scale FeNb conversion facility in 1971 (SLC, 1971). Thereafter, the company marketed both pyrochlore concentrate and ferroniobium. The company also explored opportunities to market useful mill by-products including high-purity calcite, magnetite, and apatite as a source of phosphate fertilizer and REEs (SLC, 1971).

In latter years, despite all the measures aimed at increasing the profitability of its operation, the company was struggling financially because of competition from new lower-cost and higher-grade producers in Brazil. In 1976, after a labour dispute closed the mine, SLC went into liquidation (WSP, 2018). During its 15-year life, SLC's Oka mine produced a total of 6.35 million tons of ore at an average grade of 0.46 % Nb_2O_5 (Niocan, 2010). Annual production data are summarized in Table 1. At the time of closure, reserves (noncompliant with NI 41-103) were estimated at 21.7 million tonnes of ore grading 0.44 % Nb_2O_5 (Niocan, 2010). The mining rights to the property are currently (2024) owned by Nio Métaux Stratégiques, formerly known as Niocan Inc.

Table 1: Annual production statistics for the St. Lawrence Columbium and Metals Corporation mine at Oka, Quebec. Beginning in 1971, the company marketed its niobium production as Nb_2O_5 concentrate or as ferroniobium (FeNb).

Year	Ore Milled (tons)	Nb_2O_5 Produced in concentrate (lbs)	Ore Grade % Nb_2O_5	Reference
1961	n.a.*	134 006	n.a.	C&C, 1965[2]
1962	172 767	775 313	0.43	SLC, 1962
1963	291 403	1 393 536	0.40	SLC, 1963
1964	321 585	2 091 725	n.a.	SLC, 1964
1965	383 553	2 203 985	0.43	SLC, 1966
1966	406 698	2 647 667	0.47	SLC, 1966
1967	369 642	2 368 225	n.a.	SLC, 1967
1968	360 194	2 005 989	n.a.	SLC, 1968
1969	475 201	3 059 052	n.a.	SLC, 1969
1970	724 345	4 886 957	n.a.	SLC, 1970
1971	408 500	n.a.	n.a.	SLC, 1971
1972	589 147	n.a.	n.a.	SLC, 1972
1973	n.a.	n.a	n.a.	
1974	n.a	n.a.	n.a.	
1975	n.a	n.a.	n.a.	
1976	n.a.	n.a.	n.a.	
Total	6 350 000	39 725 600[1]	0.46	Niocan, 2010

*n.a. Data not available

[1] Estimate of equivalent Nb_2O_5 in concentrate assuming a mill recovery of 68%

[2] Carbonneau and Caron (1965), Table VI

1.3 Critical Minerals hosted in SLC Mine Tailings

Based on previous geological and mineralogical studies of the SLC mine (Carbonneau and Caron, 1965; Gold et al., 1967), the most prospective critical elements to be found in the tailings are niobium (Nb), rare earth elements (REEs), and phosphorus (P). Although not included in Canada's list (Figure 1), P is emerging as a new critical element (Spears et al., 2022).

Niobium is used mainly as an alloying metal to increase the toughness, strength, formability, and weldability of special steels used in gas pipelines and automobile structural components. Because of its temperature stability, Nb is also used in superalloys for applications including jet engine components, gas turbines, liquid-rocket thruster nozzles, and turbo-charger systems. Small amounts of Nb alloyed with Ge, Ti, and Sn are used in superconducting magnets for particle accelerators, magnetic resonance imaging (MRI), and nuclear magnetic resonance (NMR) instruments. As lithium niobate, Nb is used extensively in mobile phones.

Rare earth elements, forming the lanthanide series, are a group of 15 elements (including Y) with similar chemical properties. Traditionally used as catalysts (La, Ce) and in glass and ceramics (La, Ce, Pr, Dy, Er, Tm), they are increasingly in demand for a wide range of advanced technology applications. In particular, REEs (Pr, Nd, Sm, Tb, Dy) are used in strong permanent magnets for low-carbon technologies such as electrical vehicle motors and wind turbine generators, and for portable electronics and hard-disk drives. Other REE applications include lasers (Nd, Eu, Dy, Ho, Er, Tm, Yb), fibre optics (Pr, Er), superconductors (Gd), fuel cells (Gd, Tb), medical imaging (MRI, CT, NMR, PET, X-Ray) instruments (Eu, Gd, Tb, Ho, Tm, Yb, Lu), and magnetostrictive alloys (Tb, Dy).

Because it is an essential plant nutrient, most phosphorus production is used to make agricultural fertilizers. In the form of organophosphorus compounds, P is used in plasticizers, flame retardants, pesticides, and in water treatment. As phosphoric acid, P is used as a food additive, particularly in cola drinks. Phosphorus is also used in steel production and in phosphor bronze, a special copper alloy. An increasingly important use of P is in lithium iron phosphate, or lithium ferro-phosphate (LFP), batteries (Spears et al., 2022). These batteries are being used in electric vehicles, solar-powered lighting systems, and home energy storage (backup power).

1.4 Environmental and Social Governance Context

This study complements previous GSC investigations on the geoenvironmental signature of mine wastes and contact waters at the SLC site performed under the Environmental Geosciences Program (EGP) between 2016 and 2018 (Desbarats et al., 2020a; 2020b; 2022; 2024). In particular, the GSC investigated the mineralogy, pore-water chemistry, and seepage chemistry of impounded tailings (Desbarats et al., 2020a; Desbarats et al., 2022). Some of the results presented herein are reproduced from these earlier reports. The Ministère de l'Énergie et des Ressources Naturelles du Quebec (MERNQ) carried out characterization studies of mine wastes in support of its ongoing site remediation activities (WSP, 2018). The site lies within the boundaries of the municipality of Oka, which currently (2024) owns the property. The Mohawks of Kanesatake are the nearest Indigenous community. Engagement with provincial, municipal, and indigenous stakeholders started with the original EGP project and is continuing. Agriculture is the most important land use in the study area, with numerous apple orchards, market gardens, and vineyards. Maple sugar bushes are found on the wooded hills. Because of its proximity to the Greater Montréal Area, farmland around Oka is threatened by urban expansion.

1.5 Objectives and Scope

The first objective of the Critical Minerals Geoscience and Data Program (CMGD) is to develop a critical mineral knowledge base through comprehensive sampling and analysis activities to characterize critical mineral contents and associations within Canada's mineral deposits and derivative products (ores, concentrates, minerals, tailings, and wastes). All data generated by these activities are made freely available to the public. To address the CMGD objective, this study presents the results of systematic sampling and analyses of tailings at the former SLC mine, which produced Nb from a carbonatite-hosted Nb-REE deposit. Specific objectives of this study are to answer the following questions:

1. What are the physical characteristics of the mine tailings, including their granulometry, density, and moisture content?

2. What minerals are found in the tailings, including those that host critical elements and those that are potentially deleterious for re-processing?

3. What are the compositions of minerals hosting the critical elements of interest?

4. What are the concentrations of critical elements in the tailings?

5. What are the potential critical mineral resources contained in the SLC tailings?

The scope of this report is limited to geoscience aspects of critical minerals found in the SLC mine tailings. The technical and economic feasibility of re-processing these tailings are not addressed. Estimates of critical mineral abundances contained in the tailings are not NI 43-101 compliant and were not intended to be.

1.6 Accompanying Compact Disk

A Compact Disk (CD) accompanying this report contains four data files in Microsoft Excel® format. These files are described as follows:

- of_9185_tailings properties.xlsx: file containing tailings gravimetric water contents, densities, and grain-size analyses.
- of_9185_tailings geochemistry.xlsx: file containing tailings geochemical analyses.
- of_9185_tailings mineralogy_SEM.xlsx: file containing SEM mineralogy results.
- of_9185_tailings mineralogy_EPMA.xlsx: file containing EPMA results for pyrochlore and apatite grains.

1.7 Acknowledgments

This project was supported by the Environmental Geoscience and Critical Minerals Geoscience and Data programs of the Geological Survey of Canada (GSC). Shauna Madore and Miriam Wygergangs performed the physical measurements on tailings cores at the GSC Sedimentology Laboratory in Ottawa. X-Ray diffraction analyses were carried out by Igor Bilot. Matthew Polivchuk and Marc Beauchamp of the GSC Microbeam Facility performed the SEM-EDS and EPMA analyses, respectively. The authors would like to thank Wouter Bleeker for providing helpful comments on a draft version of this report. Permission to access the SLC site was graciously granted by the Municipality of Oka.

2. STUDY AREA

2.1 Climatic and Physiographic Setting

The former Saint Lawrence Columbium mine (lat. 45.502°; long. 74.029° W) is located near Oka, Quebec, approximately 36 km west of downtown Montréal. The village of Oka is part of the Deux Montagnes Municipalité Régionale de Comté (MRC), in the Basses Laurentides administrative region of Quebec. The mine site is readily accessed from Montréal via highways 640 and 344.

The study area falls within the "Humid Mid-Cool Temperate" (MCTh) ecoclimatic region, which is characterized by warm summers and relatively mild winters (Strong et al., 1989). Between April and November, mean daily temperatures are above 0°C. At Environment Canada's Oka weather station, 3.2 km from the mine site, the mean annual temperature is approximately 6.0°C. The mean summer (July) temperature is 20.3°C and the mean winter (January) temperature is -10.9°C. Monthly precipitation, usually in excess of 70 mm, is fairly evenly distributed throughout the year. Mean annual precipitation is approximately 1107 mm including 871 mm of rainfall and 236 mm of snowfall equivalent. Climate Normals for the Oka weather station are presented in Table 2.

The mine site lies within the Saint Lawrence Lowlands ecoregion, which includes the valleys of the Ottawa and Saint Lawrence rivers (Ecozones, 2018). Most of the lowlands are underlain by flat-lying Paleozoic strata resting on Precambrian bedrock. In the study area, however, Precambrian inliers form the Oka, Saint-André, and Rigaud Hills. Elevations range from 230 m on the highest of the Oka hills to 22 m on nearby Lac des Deux Montagnes. The landscape of the Saint Lawrence lowlands has been shaped by the last continental glaciation, followed by the Champlain Sea incursion and retreat, and subsequent river erosion and deposition. Most of the lowlands are blanketed by glacio-marine clay of the Champlain Sea, which can reach a thickness of over 60 m. More elevated areas, such as the Oka Hills, are covered by glacial till resting on bedrock. Reworking of the till by wave action during the marine retreat has left numerous sandy and cobble terraces representing former strand lines.

The west side of the mine area is drained by a ditch, which eventually joins the Ruisseau Rousse. On the east, the site is drained by a small creek known as the "effluent Saint-Pierre" (WSP, 2018). Both these water courses flow to the Grande Baie on the Lac des Deux Montagnes, which forms the confluence of the Ottawa River and the Rivière des Milles Iles.

The dominant vegetation in the ecoregion is mixed-wood forest consisting of sugar maple, yellow birch, eastern hemlock, and eastern white pine, with beech appearing on warmer sites. Dry sites are dominated by red and eastern white pine, and red oak. Wetter sites support red maple, black ash, white spruce, tamarack, and eastern white cedar. Characteristic wildlife includes white-tailed deer, black bear, raccoon, skunk, squirrel, and chipmunk (Ecozones, 2018).

Table 2: Climate Normals (1981-2010) for the weather station at Oka, Quebec (lat. 45° 30.00', lon. 74° 04.00' W, elevation 91.4 m asl). Data from ECCC (2018).

Month	Daily Average (°C)	Daily Maximum (°C)	Daily Minimum (°C)	Rainfall (mm)	Snowfall (cm)	Precipitation (mm)
Jan	-10.9	-6.1	-15.7	30.2	59.9	90.2
Feb	-8.9	-3.6	-14.1	21.4	50.9	72.3
Mar	-2.9	2.1	-7.9	33.9	37.7	71.6
Apr	5.7	11.0	0.4	78.1	10.9	88.7
May	12.7	18.7	6.7	93.3	0	93.3
Jun	17.8	23.6	12.0	105.4	0	105.4
Jul	20.3	26.0	14.6	97.5	0	97.5
Aug	19.0	24.9	13.2	99.9	0	99.9
Sep	14.5	20.3	8.8	95.3	0	95.3
Oct	7.7	12.6	2.8	102.6	2.5	105.1
Nov	1.3	5.1	-2.5	78.0	20.0	97.9
Dec	-6.4	-2.2	-10.4	35.3	54.3	89.6
Year	**5.8**	**11.0**	**0.6**	**871**	**236**	**1107**

2.2 Geological Setting

The Oka Carbonatite Complex has been studied extensively because of its rare and unusual rock types and minerals (Gold et al., 1967; Gold and Vallée, 1969; Eby, 1975; Treiman and Essene, 1985; Hornig-Kjarsgaard, 1998; Chen and Simonetti, 2013; 2014). A brief overview of the geology of the complex and of the SLC mine is provided here based on these references.

The Cretaceous (113-127 Ma) Oka Carbonatite Complex belongs to the suite of alkaline intrusions that form the Monteregian Hills. It was emplaced within a Precambrian inlier of Grenville gneisses and anorthosites metasomatically altered (fenitized) locally in contact with the intrusion. The inlier is surrounded by gently dipping basal Paleozoic strata represented by Potsdam Group conglomerates and sandstones of the Cambrian Covey Hill and Cairnside Formations.

The Oka Complex consists of two ring-shaped structures forming a distorted "figure 8" 7.2 km long by 2.4 km wide and aligned in a NW-SE direction (Figure 2). The carbonatites are intercalated with ring-dykes and cone-sheets of silica-undersaturated alkaline rock types and ultramafic units. The main geological units within the complex belong to four distinct series:

- Carbonatites. Most of the carbonatite, including the core of the complex, consists of a coarse-grained calcite-carbonatite (sövite) although dolomite-carbonatite (rauhaugite) is found in the northwest of the complex. The sövites typically contain 70-90 % calcite and variable amounts of accessory biotite, sodian augite, richterite, apatite, nepheline, monticellite, melilite, magnetite, perovskite, pyrochlore, niocalite, pyrite, and pyrrhotite.
- Melteigite-Ijolite-Urtite series. Rocks of this series are composed of nepheline and variable amounts of mafic minerals such as alkali pyroxene and amphiboles, biotite, and melilite. Urtite contains over 70% nepheline whereas melteigite, the mafic end-member, consists mostly of pyroxenes. Most rocks are ijolites containing up to 50 % nepheline.
- Okaite-Jacupirangite series. These ultramafic rocks are composed essentially of melilite, hauyne, and pyroxene with accessory biotite, perovskite, apatite, magnetite, and calcite. Within the complex, the series exhibits considerable compositional variation.
- Alnoites. Alnoite and breccias with an alnoite matrix form late-stage dykes and plugs around the complex and in the surrounding gneisses. Alnoites are porphyritic ultramafic rocks containing phenocrysts of biotite or phlogopite, augite, olivine, and magnetite in a matrix of melilite, phlogopite, perovskite, calcite, and apatite. Here, the melilite has been replaced by calcite and perovskite is largely absent.

2.3 Economic Geology

All rock types within the Oka complex contain some degree of primary Nb mineralization of magmatic origin. However, sövites are the main economic host of Nb. The SLC mine was developed within the "A" zone (Figure 3), which consists of sövites intruded by tabular bodies and irregular masses of ijolite, and some okaite (Gold et al., 1967). The main constituents of the sövites are calcite (70-85 wt.%) and apatite (4-15 wt.%), with variable amounts of biotite (3-15 wt.%), pyroxene (0-11 wr.%), monticellite (0-10 wt.%), magnetite (0.5-5 wt.%), and sulfides (1-3 wt.%)

mainly as pyrite, pyrrhotite or sphalerite, and pyrochlore (0-1 wt.%). Pyrochlore, the main Nb-bearing mineral, appears to have a particular affinity for sövites rich in apatite, magnetite, pyroxene, and monticellite. However, because all sövites contain some pyrochlore, ore-waste limits were essentially economic, and mining required stringent grade control measures according to sövite type. Based on mineralogy and mill performance, sövite ores were classified into five different types (Carbonneau and Caron, 1965):

A. High-calcite sövite (80 % calcite; 8 % apatite; 0.9 % pyrochlore)
B. Monticellite sövite (76 % calcite; 5 % apatite; 10 % monticellite; 0.8 % pyrochlore)
C. Pyroxene sövite (70 % calcite; 8 % apatite; 11 % pyroxene; 1.9 % pyrochlore)
D. Ijolitic sövite (65 % calcite; 7 % apatite; 15 % biotite; 1.4 % pyrochlore)
E. Chloritized and leached sövite (50 % calcite; 4 % apatite; 30 % chlorite; 1.0 % pyrochlore)

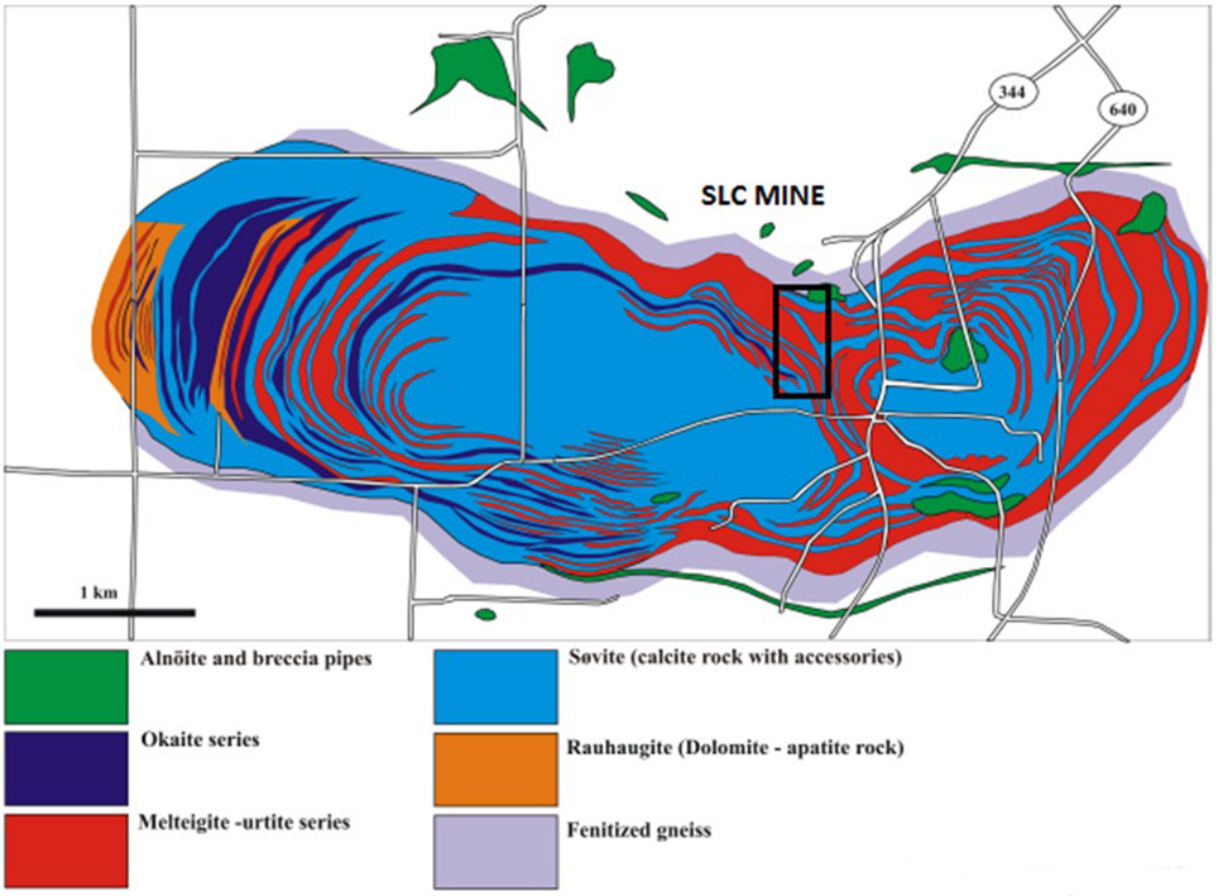

Figure 2: Simplified geology of the Oka Complex (modified from Figure 11 of Lentz et al., 2006). The black rectangle indicates the location of the SLC site.

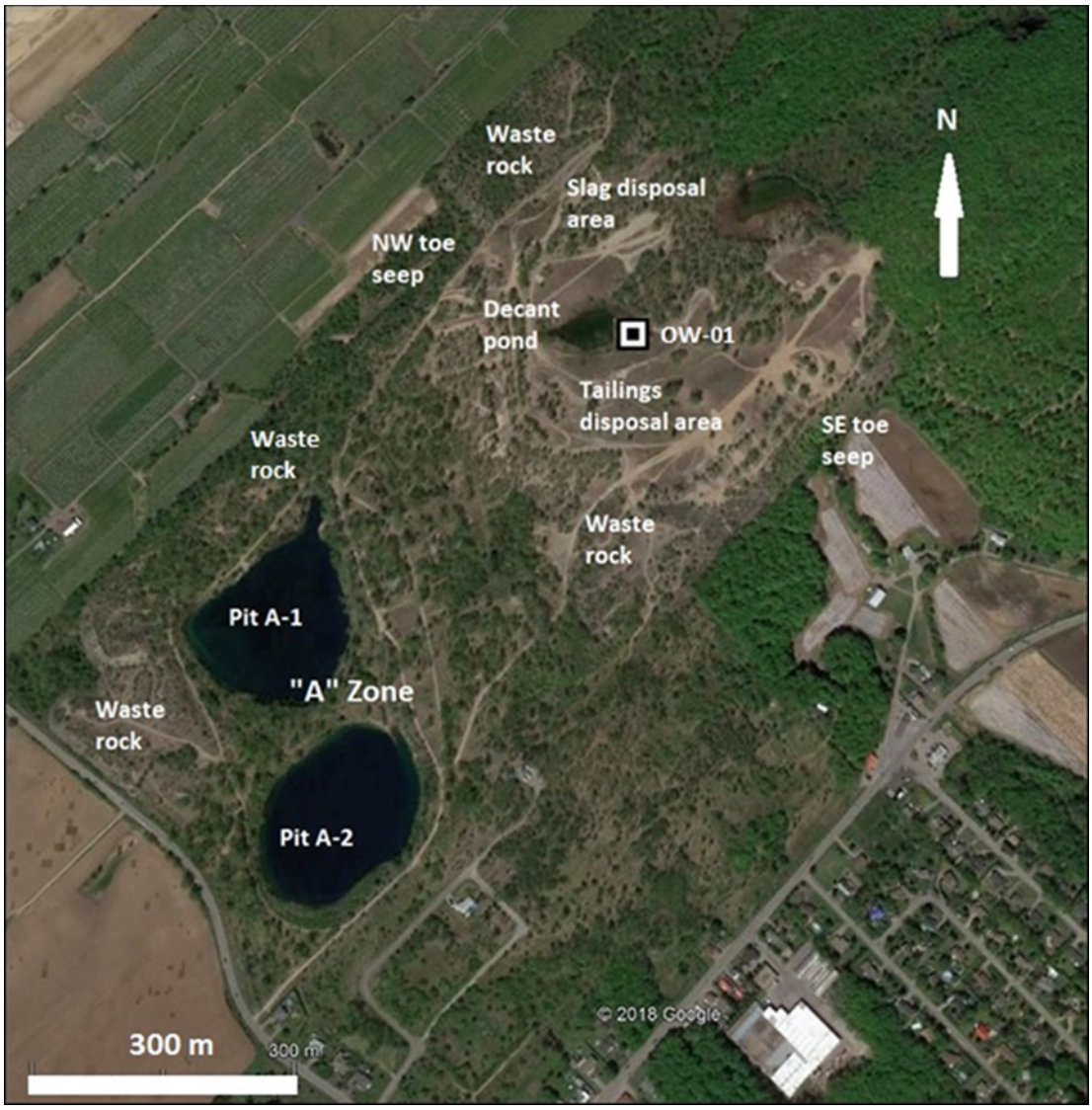

Figure 3: Satellite image with annotations showing the main features of the former SLC mine site in 2018 as well as the location of the GSC study site and stratigraphic borehole (OW-01). The borehole coordinates are longitude -74.02628° W and latitude 45.50450° N. Google Earth Image used with permission.

Pyrochlore is a niobium oxide having the general formula (Zurevinski and Mitchell, 2004): A_{16-x} B_{16} O_{48} $(O,OH,F)_{8-y}$: z H_2O where x and y are vacant sites in the unit cell. The pyrochlore structure can accommodate a wide variety of cations in the *A* and *B* sites. At the SLC mine, *A* site cations may include Ca, Na, REEs, U, Th, Sr, Mn, and Y whereas the *B* sites are occupied mainly by Nb, with Ti, Ta, Zr, and Fe (Gold et al., 1967). Because of these substitutions, pyrochlore compositions are extremely variable at the SLC mine and elsewhere within the Oka complex (Carbonneau and Caron, 1965; Gold et al., 1967; Petruk and Owens, 1975; Zurevinski and Mitchell, 2004). Pyrochlores in unaltered sövites contain from 47 to 66 wt.% Nb_2O_5. Primary pyrochlore may also contain up to 0.72 wt.% U_3O_8 and 1.51 wt.% ThO_2 (Carbonneau and Caron, 1965). Deuteric pyrochlore is found in hydrothermally altered and biotitized zones. Although Nb grades may be higher in these zones they were avoided because the ore responded poorly to the milling process. Deuteric pyrochlore may contain up to 1.83 wt.% U_3O_8 and 7.23 wt.% ThO_2 (Gold et al., 1967). Uranian pyrochlore and uranopyrochlore from the SLC mine may contain up to 15.11 wt.% and 24.79 wt.% U_3O_8, respectively (Petruk and Owens, 1975). Other Nb-bearing phases uniquely found within the Oka complex are perovskite (latrappite) and niocalite (Gold et al., 1967). However, neither mineral is of economic significance. Pyrochlores from the SLC mine also contain rare earth concentrations of up to 11.1 wt. % ΣREEO (Gold et al., 1967; Petruk and Owens, 1975).

Calcite and apatite are important gangue minerals in the deposit. Previous research has shown that they both contain elevated concentrations of REEs, apatite in particular (Eby, 1975; Hornig-Kjarsgaard, 1998; Chen and Simonetti, 2013).

2.4 Ore Processing

Production of a marketable pyrochlore concentrate was challenging due to the variable composition of the ore and the milling process required continual improvement throughout the mine life aimed at increasing recovery efficiency (Carbonneau and Caron, 1965; Gibson et al., 2015). Carbonneau and Caron (1965) provide a relatively detailed description of the SLC milling process as it was in the early years of production. Their description is summarized here with a view toward identifying the various waste streams reporting to the tailings disposal area.

The composition of the ore feed was approximately 0.8-1.9% pyrochlore, 50-80% calcite, 4-8% apatite, 0-11% pyroxene, 3-15% micas, 2-3% magnetite, 1-3% sulfides (pyrite, pyrrhotite, sphalerite), and 1-30% other silicates including chlorite. After crushing, grinding, and desliming, the ore was fed to a sulfide flotation circuit for removal of pyrite, pyrrhotite, and sphalerite. The tailings from this circuit were sent to a magnetic separator for recovery of a magnetite by-product and additional pyrrhotite. The resulting non-magnetic concentrate was deslimed by cycloning and was then sent to a rougher bulk flotation circuit. The tailings from this circuit were sent to a cyclone with coarse particles being sent to the tailings impoundment and calcite fines being recovered for marketing as agricultural lime. The concentrate from the rougher circuit contained most of the pyrochlore as well as silicates and some apatite. After further desliming and magnetic separation steps, this concentrate was sent to a two-stage cleaning circuit in which pyrochlore was first floated from apatite under neutral pH and then from micas and other silicates under acidic conditions promoted by the addition of hydrofluoric acid. Remaining silicates and sulfides in the concentrate were removed through two reverse flotation stages in series. The final concentrate was composed

of 92-98% pyrochlore (Gold and Vallée, 1969) and contained on average 60% Nb_2O_5 (Gold et al., 1967, Table IV). The recovery efficiency was variable according to ore classification. Higher recoveries were achieved for ores with greater calcite and lower mica contents (Carbonneau and Caron, 1965; Gold et al., 1967). While the target efficiency was 80%, the actual efficiency was about 10% lower due to the variability of the mill feed (Carbonneau and Caron, 1965). Based on this information and on production figures, Niocan (2010) estimated recovery at 68%.

The types of mill waste sent to the tailings disposal area included float from the sulfide recovery circuits, coarse tailings from the rougher circuit and fines from desliming and the cleaning circuits. The sulfide float was composed mainly of pyrite, pyrrhotite, and sphalerite. The coarse tailings were composed mainly of calcite and apatite. The finer tailings and slimes contained biotite, apatite, chlorite, and pyroxene.

2.5 Tailings Disposal

Tailings from the SLC mill were deposited within a topographic saddle bounded to the northeast by the rising terrain of St-Joseph-du-Lac hill and to the southwest by a low knoll (Figure 3). On the northwest and southeast sides of the impoundment, the saddle was bridged by steep berms constructed from waste rock and coarse tailings in two lifts using the upstream method. The tailings disposal area covers approximately 19.24 ha and has an estimated volume of 1,396,510 m^3 (WSP, 2018). This estimate was based on sparse information from partially-penetrating boreholes. Here, the tailings volume is estimated from mine production figures (Table 1). Assuming 5,760,720 metric tonnes of ore milled (6,350,000 tons), an average tailings solids density of 2.82 tonnes/m^3, an average porosity of 0.47 (Section 4.1), and neglecting the weight of recovered pyrochlore, the volume of tailings emplaced in the impoundment was about 3,854,400 m^3. This is more than double the volume estimated by WSP (2018). Given an area of 19.24 ha, the average thickness of the impoundment would be about 20 m. In the central basin of the impoundment, the thickness of tailings reaches 24.5 m at the GSC stratigraphic borehole (Section 4.1) and 29.6 m at MERN borehole PO-13 (WSP, 2018). The tailings thickness tapers to zero on the northeast edge of the impoundment.

An air photo of the tailings impoundment as it was in 1965 (Figure 4) shows that it was subdivided internally into sub-basins by several dikes. The different colours within each sub-basin suggest that they received different waste streams from the mill. One of the sub-basins likely served as a decant pond for recycling process water to the mill. By 1975, the internal configuration of the impoundment had changed radically, with new dikes partially enclosing what is likely a decant pond (Figure 5). Berms of coarse white calcite-rich tailings are seen on the northwest and southeast sides of the impoundment. These two photographs illustrate how tailings management varied over the mine life. Disposal of tailings into different sub-basins separated by dikes, changing slurry spigot locations, and density and textural segregation are all factors that impart considerable heterogeneity within the impoundment. This heterogeneity complicates the assessment of potential unrecovered mineral resources contained within the tailings.

Figure 4: Air photo of the SLC mine site showing the tailings impoundment (upper right) as it was in June 1965. Note the apple orchard being gradually buried by the tailings. National Air Photo Library photo A18763-206 (detail) used with permission.

Figure 5: Air photo of the SLC mine site showing the tailings impoundment (upper right) as it was in June 1975. National Air Photo Library photo A23966-082 (detail) used with permission.

3. METHODOLOGY

3.1 Borehole Site Selection and Drilling

A stratigraphic borehole (OW-01) was sited next to the decant pond, in the central basin of the impoundment pond, where the tailings accumulation was believed to be thickest (Figure 3) The borehole was drilled through the entire tailings accumulation to obtain a detailed and representative vertical profile of tailings textural, mineralogical, and geochemical variations. Drilling was performed on September 20th, 2018, by George Downing Estate Drilling Ltd. using a Central Mine Equipment (CME) Model 55 track-mounted rig. Hollow-stem augering (Figure 6) was used to 7.6 m (25 ft.). Because of the increasingly soft nature of the fine-grained saturated tailings, the drilling method then was switched to direct circulation with casing advancement (Figure 7) until the end of hole at 25 m (80 ft.). Split-spoon core samples were obtained at regular 0.75 m (2.5 ft.) intervals throughout the tailings sequence by driving a 2 in. x 24 in. split-tube sampler. Photographs of each core sample can be found in the Appendix of Desbarats et al. (2020a).

3.2 Laboratory Methods

Tailings granulometry and physical properties

Tailings grain-size, density, and natural water content analyses were performed at the GSC Sedimentology Laboratory in Ottawa. For class sizes greater than 63 µm, grain-size measurements were made using wet sieving followed by dynamic image analysis (Microtrac Camsizer ®). For class sizes smaller than 63 µm, grain-sizes were determined by laser diffraction particle sizing (Beckman-Coulter LS 13-320 ®). Densities were measured on oven-dried samples using a Micromeritics AccuPyc 1330 ® gas displacement pycnometer. Gravimetric (or natural) water contents of the tailings samples were measured according to ASTM-D2216. Gravimetric water content (W_N) is defined as the ratio of the mass of water contained in the pore spaces of the material to the solid mass of particles, expressed as a percentage. Atterberg limits (liquid and plastic) and derived indices for the samples were determined following ASTM-D4318. The liquid limit (W_L) is defined as the water content (%) of the tailings at the boundary between semiliquid and plastic states. The plastic limit (W_P) is defined as the water content (%) at the boundary between plastic and semi-solid states. The plasticity index (%) is the range of water contents over which the tailings behave plastically and is equal to the liquid limit minus the plastic limit (W_L-W_P). The liquidity index (%) is defined as $(W_N – W_P) / (W_L – W_P)$ or the ratio of the water content minus the plastic limit to the plasticity index.

X-ray Diffraction

Quantitative mineralogical analyses of tailings samples were conducted by X-ray diffraction (XRD) at the GSC Mineralogy X-Ray Laboratory. Bulk materials were pulverized to < 10 µm using a McCrone micronizing mill and used to prepare uniform, randomly-oriented pressed powder mounts. X-ray patterns were captured using a Bruker D8 Advance Powder Diffractometer equipped with a Lynx-Eye Detector and Co Kα radiation set at 35 kV and 35 mA. Initial identification of minerals was made using EVA (Bruker AXS Inc.) software with comparison to

reference mineral patterns using Powder Diffraction Files of the International Centre for Diffraction Data and other databases. Quantitative analysis of the pressed powder mounts was completed using Rietveld Refinement (TOPAS software, Bruker AXS Inc.), based on a whole pattern-fitting algorithm. Results are reported in wt. %. The detection limit is about 3 wt.%.

Scanning Electron Microscopy

To identify trace minerals in the tailings samples, Energy Dispersive X-ray Spectroscopy (EDS) analyses were conducted on individual grains using an SEM. To prepare suitable samples for SEM analysis, a very dilute suspension of the samples was prepared in distilled water and pipetted onto a piece of carbon tape affixed to an aluminum pin stub and left to dry. SEM-EDS analyses were performed at the GSC on a Zeiss EVO50 environmental SEM equipped with an X-Max 150 silicon drift detector from Oxford Instruments. The samples were imaged in backscattered electron (BSE) mode and selectively analyzed based primarily on differences in their brightness, which reflects compositional differences. Manual interpretation of the mineralogy was then done based on the generated spectra. Analytical conditions included a chamber pressure of 10 Pa, accelerating voltage of 20 kV, working distance of 8.5 mm, and probe current of approximately 0.75 nA. Spot EDS analyses were collected for a live time of 3 s with the software process time set to 3.

Electron Probe Microanalyses

Tailings samples from the >63 μm and the >2 μm size fractions were prepared into 25 mm round epoxy grain mounts using West System® epoxy resin. Upon curing, they were progressively smoothed to a 1 μm final polish using a Buehler Ecomet 30 polisher. Stitched backscattered electron images of the polished epoxy grain mounts were collected using the Aztec software by Oxford Instruments using a Tescan Mira3 field emission scanning electron microscope at the GSC Microbeam Laboratory. Analyses were conducted using a JEOL-8230 electron probe microanalyzer, equipped with 5 wavelength dispersive spectrometers. Operating conditions were 20 kV accelerating voltage, 20 nA beam current, and spot size of 1 um. Calibration standards consisted of pure elements, and well-characterized natural and synthetic minerals. Counting times were 20 seconds on peak and 10 seconds on each background for all elements except Si, Na, and F, which were 30 seconds on peak and 15 seconds on each background. Several overlap corrections were necessary to correct for peak overlaps, principally in the rare-earth elements. Matrix corrections were accomplished using the default JEOL ZAF correction routine.

Tailings geochemistry

Analyses of tailings bulk chemistry were performed by Bureau Veritas Commodities Canada Ltd. in Vancouver. Measurements were made using lithium borate fusion with Inductively Coupled Plasma - Emission Spectroscopy (ICP-ES) for whole rock analyses and most minor elements, and Inductively Coupled Plasma - Mass Spectrometry (ICP-MS) for trace elements. Aqua Regia digestion with ICP-MS was used for Mo, Cu, Pb, Zn, Ni, As, Cd, Sb, Bi, Ag, Au, Hg, Tl, and Se. Fluorine was determined using hydropyrolysis and ion chromatography. Certified reference materials included a silica blank, GSR-6, and Oka-1 (Steger and Bowman, 1981).

Figure 6: Drilling of the stratigraphic borehole by hollow-stem augering. Photograph by J.B. Percival. NRCan Photo Database number 2020-637.

Figure 7: Drilling of the stratigraphic borehole by casing advancement. Photograph by J.B. Percival. NRCan Photo Database number 2020-638.

4. RESULTS

4.1 Tailings Physical Properties

The tailings samples from the GSC stratigraphic borehole exhibit a continuum of textures varying between sand and clayey silt (Figure 8a). The vertical succession of these textures (Figure 8b) illustrates the physical heterogeneity of tailings within the impoundment. A 4.4 m layer of silty sand blankets the base of the impoundment. This unit is overlain by 17.5 m of silts and clayey silts with a few interbedded sandy horizons. The whole sequence is capped by 2.6 m of coarse sand. Whereas fine-textured tailings are expected in the central basin of the impoundment near the decant pond, these coarse tailings are not. This material is believed to have been bulldozed inward from tailings beaches on the periphery of the impoundment as a dust suppression measure in the 1980s (WSP, 2018). Complete grain-size distribution data can be found in an accompanying digital file.

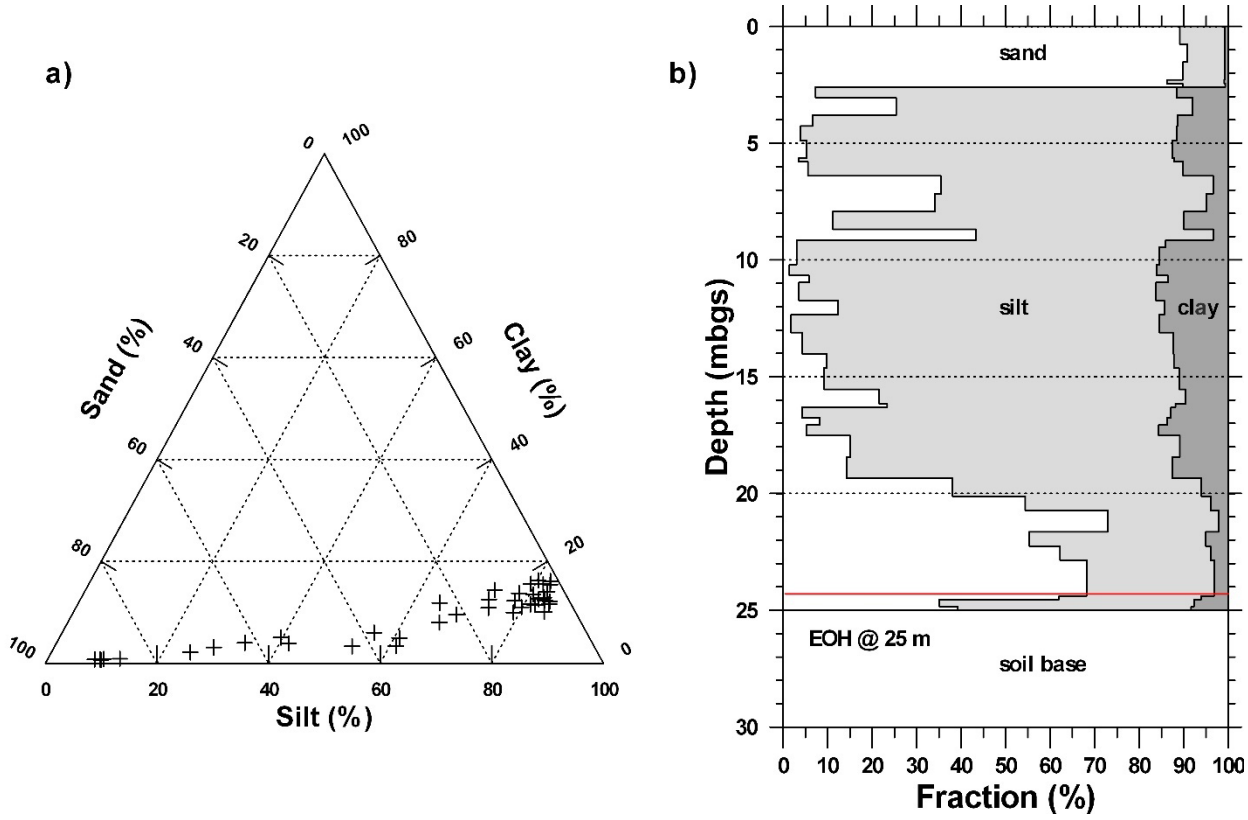

Figure 8: Ternary plot of textures observed in split-spoon samples. Clay defined as particles less than 2 µm (a); Downhole textural variations of tailings in the GSC stratigraphic borehole (b). Red line marks the base of the tailings

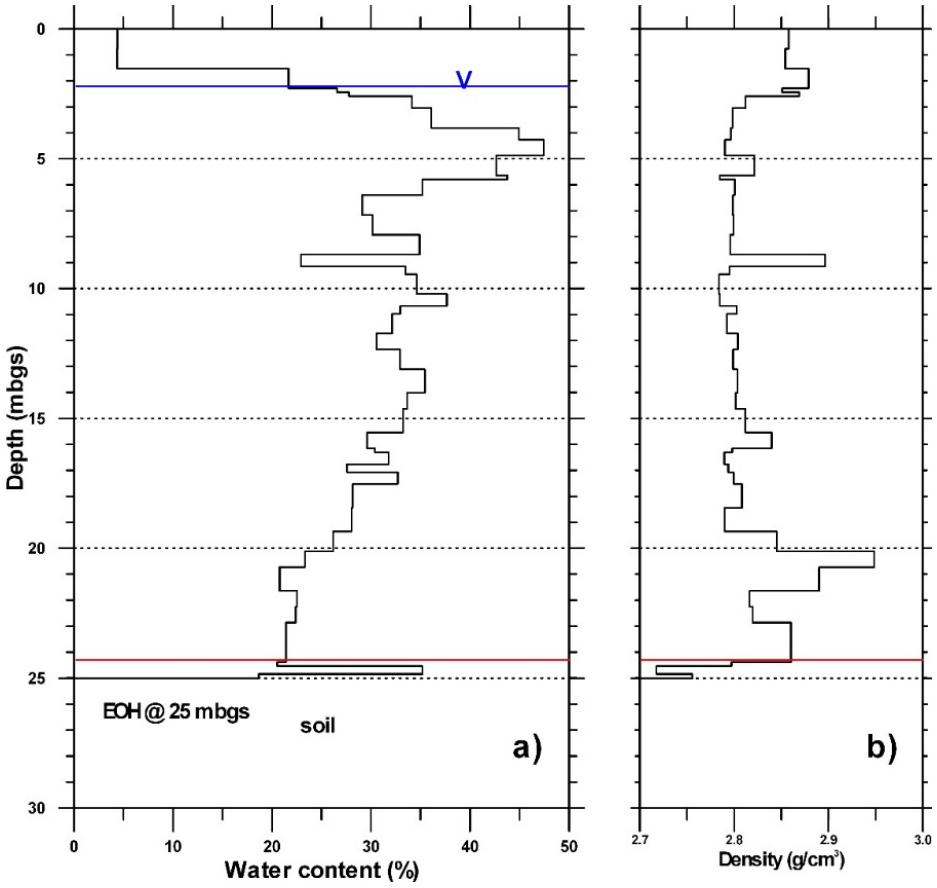

Figure 9: Downhole profiles of gravimetric water content (a) and density (b) in the GSC stratigraphic borehole. The approximate depth of the water table is marked by a "V" on the water content profile. The base of the tailings is marked by a red line.

Across the unsaturated zone, water content increases with depth from 4% to 22% (Figure 9a). The depth of the water table is approximately 2.2 m. Below the water table, saturated water contents vary between 47% in a clayey silt layer 4 m below ground surface to 20% in the sandy layer at the base of the impoundment (Figure 9a; Table 3). The higher water contents in near-surface fine tailings likely reflect a lower degree of consolidation compared to fine tailings at depth. Average water content is 30 %. Tailings solids densities are generally between 2.8 and 2.9 g/cm^3 (Figure 9b) with an average of 2.82 g/cm^3. The depth profile illustrates density segregation in a few discrete horizons. Density spikes at depths of 9 and 20 m reflect larger amounts of apatite, magnetite, and possibly sulphides, in the tailings. Porosity values calculated from saturated water contents and densities are reported in Desbarats et al. (2020a). The average tailings porosity is 47%.

Atterberg limits (liquid, plastic) measured on tailings samples and derived indices are presented in Table 3. The mean plasticity index of fine-grained tailings is 11.3% (medium plastic). The liquidity index of most of these tailings is 1 (very soft).

Table 3: Atterberg limits. Shaded samples are in the soil underlying the tailings.

Sample No.	Depth from (m)	Depth to (m)	Water Content (%)	Liquid Limit (%)	Plastic Limit (%)	Plasticity Index (%)	Liquid. Index (%)	Plastic. Class.
DUA-18-T1	0.00	0.61	4.4	TS	-	-	-	-
DUA-18-T2	0.76	1.37	4.4	TS	-	-	-	-
DUA-18-T3	1.52	2.13	21.7	TS	-	-	-	-
DUA-18-T4A	2.29	2.44	26.6	IN	-	-	-	-
DUA-18-T4B	2.44	2.59	27.8	TS	-	-	-	-
DUA-18-T4C	2.59	2.90	34.2	IN	-	-	-	-
DUA-18-T5	3.05	3.66	36.1	IN	-	-	-	-
DUA-18-T6A	3.81	4.27	44.9	44.1	27.4	16.7	1	ML
DUA-18-T6B	4.27	4.42	47.5	TS	-	-	-	-
DUA-18-T7	4.88	5.18	42.6	34.2	23.7	10.5	2	CL
DUA-18-T8A	5.64	5.79	43.8	33.7	24.5	9.2	2	ML
DUA-18-T8B	5.79	5.94	35.2	35.4	23.5	12.0	1	CL
DUA-18-T9	6.40	6.71	29.1	TS	-	-	-	-
DUA-18-T10	7.16	7.47	30.1	TS	-	-	-	-
DUA-18-T11	7.92	8.23	34.9	35.7	24.2	11.5	1	CL
DUA-18-T12	8.69	8.99	22.9	IN	-	-	-	-
DUA-18-T13A	9.14	9.45	33.5	34.3	23.0	11.3	1	CL
DUA-18-T13B	9.45	9.75	34.6	33.4	24.0	9.4	1	ML
DUA-18-T14	10.21	10.52	37.7	38.0	24.9	13.0	1	ML
DUA-18-T15A	10.67	10.97	33.0	33.3	23.5	9.8	1	CL
DUA-18-T15B	10.97	11.28	32.1	38.3	24.9	13.3	1	ML
DUA-18-T16	11.73	12.04	30.6	36.7	23.7	13.1	1	CL
DUA-18-T17	12.34	12.65	32.9	38.1	24.7	13.4	1	CL
DUA-18-T18	13.11	13.41	35.5	41.3	25.2	16.1	1	CL
DUA-18-T19	14.02	14.33	33.6	TS	-	-	-	-
DUA-18-T20	14.63	14.94	33.3	32.7	25.0	7.8	1	ML
DUA-18-T21	15.54	15.85	29.6	33.8	23.1	10.7	1	CL
DUA-18-T22A/B	16.15	16.61	31.1	IN	-	-	-	-
DUA-18-T23A/B	16.76	17.37	32.7	29.7	22.4	7.3	1	CL
DUA-18-T24	17.53	18.14	28.2	INS	-	-	-	-
DUA-18-T25	18.44	18.75	28.0	28.8	22.0	6.8	1	CL-ML
DUA-18-T26	19.35	19.66	26.2	TS	-	-	-	-
DUA-18-T27	20.12	20.42	23.3	TS	-	-	-	-
DUA-18-T28	20.57	21.18	20.8	IN	-	-	-	-
DUA-18-T29	21.34	21.95	22.5	IN	-	-	-	-
DUA-18-T30	22.25	22.56	22.4	IN	-	-	-	-
DUA-18-T31	22.86	23.47	21.4	IN	-	-	-	-
DUA-18-T32A	24.38	24.54	20.5	IN	-	-	-	-
DUA-18-T32B	24.54	24.84	35.2	32.6	20.7	11.9	1	CL
DUA-18-T32C	24.84	25.05	18.7	IN	-	-	-	-

TS: too sandy; IN: insufficient sample; liquidity index = 1 (very soft); liquidity index = 2 (liquid when disturbed); plasticity index < 7 (low plastic); plasticity index 7-17 (medium plastic); plasticity classification = ML (silt); plasticity classification = CL (lean clay).

4.2 Tailings Mineralogy

Recovery of critical metals from tailings requires a detailed characterization of their mineral hosts as well as an understanding of other phases that may complicate reprocessing or pose an environmental risk. This section presents mineralogical observations (XRD, SEM, EPMA) on tailings samples from across the entire thickness of the SLC impoundment.

4.2.1 X-ray Diffraction

Minerals identified by bulk X-ray diffraction (XRD) on tailings samples are listed in Table 4 along with their estimated average abundances (wt.%) and ideal compositions. Depth profiles of abundances for the four most common minerals are shown in Figure 10. This figure reveals zonation patterns related to textural and density variations across the tailings sequence. The coarse tailings at the base of the impoundment are characterized by large amounts of apatite. The overlying fine tailings are enriched in biotite and chlorite whereas the coarse tailings capping the impoundment contain little or no chlorite. Tables 5 and 6 present a detailed description of mineral abundances in bulk tailings and in the clay size-fraction, respectively. Calcite is the dominant mineral by far (64-89 wt.%) and is distributed fairly evenly throughout the thickness of the impoundment (Figure 10, Table 5). The most important silicate mineral is biotite. Its abundance varies within the tailings and in some layers, it reaches 17 wt.% (Table 4). Fluorapatite is the third most abundant mineral, reaching up to 22 wt.% in the basal coarse tailings layer (Figure 10, Table 4). Chlorite, smectite, and kaolinite are detected across the thickness of the impoundment, mainly in the clay size fraction of the fine tailings interval (Figure 10, Tables 5 and 6). Dolomite (ferroan) is present in small amounts. Nepheline, in minor to trace amounts, is distributed fairly uniformly. Other minerals detected by bulk XRD include monticellite and magnetite (Table 5). Pyrite (5 wt.%) and clinopyroxene (3 wt.%) were found in sample DUA-18-T28 and perovskite (1 wt.%) was found in sample DUA-18-T29 (not shown). In the clay size-fraction, perovskite and gypsum were noted (Table 6). The last three samples in Tables 6 and 7 (shaded) are from the underlying soil and their mineralogy is dominated by quartz, plagioclase, and K-feldspar (not shown).

4.2.2 Scanning Electron Microscopy

To identify trace minerals, Scanning Electron Microscopy (SEM) analyses were conducted on samples across the tailings thickness. Minerals identified by SEM are documented in an accompanying digital file. Table 7 provides a summary of these minerals, as well as those previously identified by XRD. Their abundances are estimated qualitatively based on the relative frequency of their detection. Tables 8, 9, and 10 present selected minerals identified by SEM according to sample depth.

Table 4: Summary of minerals found in SLC tailings based on bulk XRD analyses. Abundances are expressed as a weight % of minerals present above the XRD detection limit.

Mineral	Modal abundance (% weight)			Ideal Formula
	Min.	Max.	Mean	
biotite	6	17	11	$K(Mg,Fe)_3AlSi_3O_{10}(F,OH)_2$
calcite	64	89	81	$CaCO_3$
chlorite	0	5	1	$(Fe,Mg,Al)_6(Si,Al)_4O_{10}(OH)_8$
dolomite	0	1	tr	$Ca(Fe,Mg,Mn)(CO_3)_2$
fluorapatite	2	22	5	$Ca_5(PO_4)_3(F,OH)$
gypsum	0	tr	tr	$CaSO_4 \cdot 2H_2O$
kaolinite	0	tr	tr	$Al_2(OH)_4Si_2O_5$
magnetite	0	1	tr	Fe_3O_4
monticellite	0	1	tr	$CaMgSiO_4$
nepheline	0	2	1	$(Na,K)AlSiO_4$
pyrite	0	5	tr	FeS_2
perovskite	0	1	tr	$CaTiO_3$
smectite	0	4	tr	$(Na,Ca)_{0.33}(Al,Mg)_2(Si_4O_{10})(OH)_2 \cdot nH_2O$

tr: trace

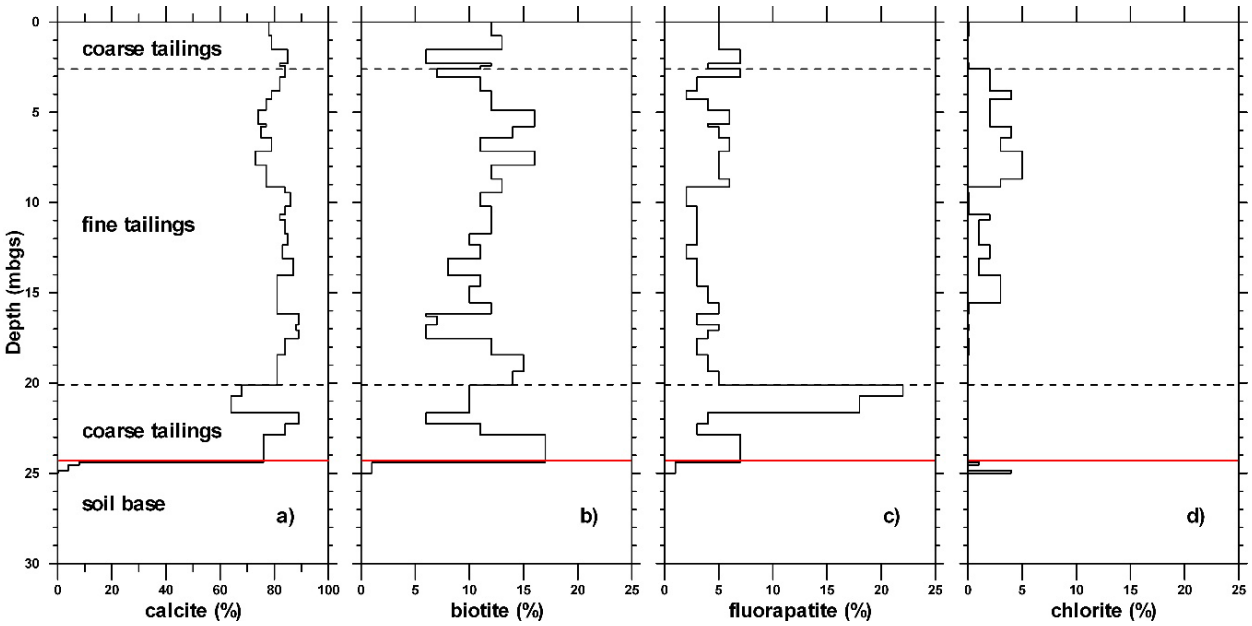

Figure 10: Mineral abundance (wt. %) depth profiles for a) calcite; b) biotite; c) fluorapatite; d) chlorite as measured by bulk XRD on split-spoon samples of tailings from the stratigraphic borehole. The dashed lines mark the top and bottom of the fine tailings interval. The red line marks the base of the tailings. (Figure S.6 from Desbarats et al., 2022)

Table 5: Quantitative mineralogy (wt. %) of bulk powdered tailings samples by XRD analyses. Shaded samples are in the soil underlying the tailings. (Table 6 from Desbarats et al., 2020a).

Sample No.	Depth from (m)	Depth to (m)	Cal	Dol	Bio	Chl	Sme	Kln	Mtc	Nph	Mag	Fap
DUA-18-T1	0.00	0.61	78	tr	12	tr	4	-	-	1	-	5
DUA-18-T2	0.76	1.37	79	tr	13	-	2	-	-	1	-	5
DUA-18-T3	1.52	2.13	85	tr	6	-	2	-	-	-	-	7
DUA-18-T4A	2.29	2.44	82	1	12	tr	1	-	-	-	tr	4
DUA-18-T4B	2.44	2.59	84	1	11	tr	-	-	-	-	tr	4
DUA-18-T4C	2.59	2.90	84	tr	7	2	-	tr	-	-	-	6
DUA-18-T5	3.05	3.66	82	tr	11	2	1	-	-	1	-	3
DUA-18-T6A	3.81	4.27	79	1	12	4	1	tr	tr	1	tr	2
DUA-18-T6B	4.27	4.42	80	tr	10	2	-	-	1	1	-	4
DUA-18-T7	4.88	5.18	74	tr	16	2	-	-	tr	2	-	6
DUA-18-T8A	5.64	5.79	77	-	16	2	-	-	-	1	tr	4
DUA-18-T8B	5.79	5.94	75	1	14	4	-	-	-	1	-	5
DUA-18-T9	6.40	6.71	79	-	11	3	-	-	-	1	-	6
DUA-18-T10	7.16	7.47	73	-	16	5	-	-	-	1	tr	5
DUA-18-T11	7.92	8.23	77	tr	12	5	-	-	-	1	-	5
DUA-18-T12	8.69	8.99	77	tr	13	3	-	tr	-	1	tr	6
DUA-18-T13A	9.14	9.45	84	-	13	-	-	-	-	1	-	2
DUA-18-T13B	9.45	9.75	86	-	11	tr	-	-	-	1	-	2
DUA-18-T14	10.21	10.52	84	-	12	tr	-	-	-	1	-	3
DUA-18-T15A	10.67	10.97	82	1	12	2	-	-	-	tr	-	3
DUA-18-T15B	10.97	11.28	84	tr	12	1	-	-	-	tr	-	3
DUA-18-T16	11.73	12.04	85	tr	10	1	-	-	-	1	-	3
DUA-18-T17	12.34	12.65	83	1	11	2	-	-	-	1	-	2
DUA-18-T18	13.11	13.41	87	1	8	1	-	-	-	1	-	2
DUA-18-T19	14.02	14.33	81	1	11	3	-	-	-	1	-	3
DUA-18-T20	14.63	14.94	81	1	10	3	-	tr	-	1	-	4
DUA-18-T21	15.54	15.85	81	1	12	tr	-	-	-	1	-	5
DUA-18-T22A/B	16.15	16.61	86	tr	10	-	-	-	-	1	-	3
DUA-18-T23A/B	16.76	17.37	85	tr	8	tr	-	-	-	1	-	6
DUA-18-T24	17.53	18.14	84	1	12	tr	-	-	-	tr	-	3
DUA-18-T25	18.44	18.75	81	-	15	-	-	-	-	tr	-	4
DUA-18-T26	19.35	19.66	81	-	14	-	-	-	-	tr	-	5
DUA-18-T27	20.12	20.42	68	tr	10	-	-	-	-	tr	tr	22
DUA-18-T28	20.57	21.18	64	tr	10	-	-	-	-	tr	-	18
DUA-18-T29	21.34	21.95	89	tr	6	-	-	-	-	-	-	4
DUA-18-T30	22.25	22.56	84	-	11	-	2	tr	-	-	-	3
DUA-18-T31	22.86	23.47	76	tr	17	-	-	-	-	-	-	7
DUA-18-T32A	24.38	24.54	8	-	-	1	-	-	-	-	5	-
DUA-18-T32B	24.54	24.84	4	-	-	-	-	-	-	-	4	-
DUA-18-T32C	24.84	25.05	tr	27	-	4	-	-	-	-	-	-

Cal: calcite; Dol: ferroan dolomite; Bio: biotite/phlogopite; Chl: chlorite; Sme: smectite; Kln: kaolinite; Mtc: monticellite; Nph: nepheline; Mag: magnetite; Fap: fluorapatite; tr: trace; -: not detected.

Table 6: Semi-quantitative mineralogy (wt. %) of tailings clay-size (< 2 µm) fraction by XRD analyses. Shaded samples are in the soil underlying the tailings (Table 7 from Desbarats et al., 2020a).

Sample No.	Depth from (m)	Depth to (m)	Cal	Dol	Bio	Chl	Sme	Kln	Fap	Gyp	Prv
DUA-18-T1	0.00	0.61	77	1	9	tr	2	-	11	-	-
DUA-18-T2	0.76	1.37	71	1	17	-	1	-	10	-	-
DUA-18-T3	1.52	2.13	77	2	9	-	1	-	11	-	-
DUA-18-T4A	2.29	2.44									
DUA-18-T4B	2.44	2.59									
DUA-18-T4C	2.59	2.90	65	1	25	3	tr	1	5	-	-
DUA-18-T5	3.05	3.66									
DUA-18-T6A	3.81	4.27	71	2	17	5	tr	-	5	-	-
DUA-18-T6B	4.27	4.42	77	1	14	3	tr	1	4	-	-
DUA-18-T7	4.88	5.18	71	1	17	6	1	-	4	-	-
DUA-18-T8A	5.64	5.79	83	1	11	2	-	-	3	-	-
DUA-18-T8B	5.79	5.94	78	1	14	3	tr	-	4	-	-
DUA-18-T9	6.40	6.71	74	1	19	4	tr	tr	2	-	-
DUA-18-T10	7.16	7.47	78	1	17	3	tr	-	1	-	-
DUA-18-T11	7.92	8.23	76	1	18	3	-	tr	2	-	-
DUA-18-T12	8.69	8.99	75	tr	18	3	-	3	1	-	-
DUA-18-T13A	9.14	9.45	84	1	11	1	tr	tr	3	-	-
DUA-18-T13B	9.45	9.75	83	1	12	1	-	-	3	-	-
DUA-18-T14	10.21	10.52	85	1	10	2	-	tr	2	-	-
DUA-18-T15A	10.67	10.97	81	1	13	2	-	-	3	-	-
DUA-18-T15B	10.97	11.28	81	1	13	2	-	-	3	-	-
DUA-18-T16	11.73	12.04	85	1	9	2	-	-	3	-	-
DUA-18-T17	12.34	12.65	84	1	8	4	tr	tr	3	-	-
DUA-18-T18	13.11	13.41	82	1	9	4	-	-	4	-	-
DUA-18-T19	14.02	14.33	80	tr	14	3	-	-	3	-	-
DUA-18-T20	14.63	14.94	81	1	11	4	-	-	3	-	-
DUA-18-T21	15.54	15.85	78	2	13	3	-	tr	4	-	-
DUA-18-T22A/B	16.15	16.61	87	1	9	tr	-	-	3	-	-
DUA-18-T23A/B	16.76	17.37	83	1	12	1	tr	-	3	-	-
DUA-18-T24	17.53	18.14	78	1	19	-	tr	-	2	-	-
DUA-18-T25	18.44	18.75	82	1	14	tr	-	tr	3	-	-
DUA-18-T26	19.35	19.66	60	1	36	-	-	-	3	-	-
DUA-18-T27	20.12	20.42	76	1	17	-	-	-	6	-	-
DUA-18-T28	20.57	21.18	73	tr	19	1	-	tr	4	3	-
DUA-18-T29	21.34	21.95	87	tr	8	-	1	-	2	-	2
DUA-18-T30	22.25	22.56	82	1	9	1	5	-	1	tr	1
DUA-18-T31	22.86	23.47	83	tr	14	tr	-	tr	3	-	-
DUA-18-T32A	24.38	24.54	1	-	-	9	-	1	-	-	-
DUA-18-T32B	24.54	24.84	tr	-	-	7	-	-	-	-	-
DUA-18-T32C	24.84	25.05	tr	39	-	3	-	-	-	-	-

Cal: calcite; Dol: ferroan dolomite; Bio: biotite; Chl: chlorite; Sme: smectite; Kln: kaolinite; Fap: fluorapatite; Gyp: gypsum; Prv: perovskite; tr: trace; -: not detected.

Table 7: Summary of minerals identified in the SLC tailings and a qualitative measure of their relative abundance. "M" indicates a mineral detected by XRD at concentrations greater than 2 wt. % weight; "m" indicates a mineral detected by XRD at concentrations lesser or equal to 2 wt. % weight; "tr" indicates a mineral measured as trace by XRD or routinely identified by SEM; "r" indicates a mineral occasionally identified by SEM. (Table S.3 from Desbarats et al., 2022)

mineral	abundance	mineral	abundance	mineral	abundance
actinolite	r	gypsum	tr	pyrite	tr
analcime	r	hornblende	r	pyrochlore	tr
ancylite	r	illite	r	pyrrhotite	tr
andradite	r	ilmenite	r	quartz	tr
aegirine	r	kaolinite	m	richterite	tr
apatite	M	K-feldspar	tr	rhodochrosite	tr
baddelyite	r	magnetite	m	rutile	r
barite	tr	molybdenite	r	serpentine	r
biotite	M	monazite	r	smectite	m
burbankite	r	monticellite	m	sodalite	r
calcite	M	muscovite	r	sphalerite	tr
chalcopyrite	r	natrolite	r	strontianite	tr
chlorite	M	nepheline	m	thomsonite	r
clinopyroxene	tr	olivine	r	titanite	r
dolomite	m	parisite	tr	wairakite	r
diopside	tr	perovskite	tr	zeolite	r
grossular	r	plagioclase	r	zirconolite	r

A much wider range of gangue minerals is revealed by SEM (Table 7). Among oxide minerals in the tailings, unrecovered magnetite and pyrochlore are ubiquitous (Table 8). Other oxide minerals detected include Nb-rich perovskite, baddeleyite, zirconolite, rutile, and ilmenite. Pyrite is the most common sulfide mineral followed by pyrrhotite and sphalerite (Table 8). Dense oxide and sulfide minerals are particularly abundant at depths between 20 and 22 m. The same horizon also contains a large amount of apatite (Table 5).

In addition to calcite and ferroan dolomite, carbonate minerals include strontianite, rhodochrosite, parisite, burbankite, and ancylite. Parisite, a rare REE fluoro-carbonate, was detected in half the samples (Table 9). Gypsum was encountered near the top of the tailings and in the basal coarse tailings whereas barite was found in most samples (Table 9).

Among the minor silicate minerals observed, Na-rich clinopyroxenes and amphiboles (mainly richterite) were the most common (Table 10). Although it was a significant accessory mineral in sövite ore (Gold et al., 1967), monticellite was not particularly abundant. Kaolinite, smectite, and zeolites minerals (analcime, natrolite, thomsonite, wairakite) were widely distributed across the tailings thickness (Table 10).

Table 8: Tailings mineralogy by SEM. Selected oxide and sulfide minerals. Shaded samples are in the soil underlying the impoundment. Common (X); present (x); not detected (-)

Sample No.	Depth from (m)	Depth to (m)	Mag	Pcl	Prv	Pyr	Pho	Sph
DUA-18-T1	0.00	0.61	X	x	-	x	-	-
DUA-18-T2	0.76	1.37	X	x	-	x	-	-
DUA-18-T3	1.52	2.13	X	x	x	x	x	-
DUA-18-T4A	2.29	2.44	X	-	x	x	x	-
DUA-18-T4B	2.44	2.59	x	X	-	X	x	-
DUA-18-T4C	2.59	2.90	x	-	-	x	-	-
DUA-18-T5	3.05	3.66	X	x	-	x	-	x
DUA-18-T6A	3.81	4.27	-	x	-	x	-	-
DUA-18-T6B	4.27	4.42	x	x	x	x	-	-
DUA-18-T7	4.88	5.18	x	x	-	x	-	-
DUA-18-T8A	5.64	5.79	X	x	-	x	x	-
DUA-18-T8B	5.79	5.94	x	x	x	X	x	-
DUA-18-T9	6.40	6.71	x	x	-	X	x	-
DUA-18-T10	7.16	7.47	X	-	x	x	x	x
DUA-18-T11	7.92	8.23	X	x	-	x	-	-
DUA-18-T12	8.69	8.99	x	X	-	X	-	-
DUA-18-T13A	9.14	9.45	x	x	x	x	x	x
DUA-18-T13B	9.45	9.75	x	X	-	x	x	x
DUA-18-T14	10.21	10.52	x	-	-	x	x	x
DUA-18-T15A	10.67	10.97	x	X	-	x	x	X
DUA-18-T15B	10.97	11.28	x	X	-	x	x	X
DUA-18-T16	11.73	12.04	x	X	-	x	-	x
DUA-18-T17	12.34	12.65	x	X	-	x	X	x
DUA-18-T18	13.11	13.41	X	x	-	x	x	x
DUA-18-T19	14.02	14.33	x	X	-	-	-	x
DUA-18-T20	14.63	14.94	x	x	-	-	X	x
DUA-18-T21	15.54	15.85	X	X	-	X	x	-
DUA-18-T22A/B	16.15	16.61	X	X	-	x	x	x
DUA-18-T23A/B	16.76	17.37	-	X	x	X	x	-
DUA-18-T24	17.53	18.14	x	X	x	x	x	x
DUA-18-T25	18.44	18.75	x	x	x	x	x	x
DUA-18-T26	19.35	19.66	x	X	-	x	X	-
DUA-18-T27	20.12	20.42	X	X	x	X	-	x
DUA-18-T28	20.57	21.18	x	X	X	X	x	X
DUA-18-T29	21.34	21.95	x	x	-	X	x	X
DUA-18-T30	22.25	22.56	x	x	-	X	-	-
DUA-18-T31	22.86	23.47	X	X	x	X	x	-
DUA-18-T32A	24.38	24.54						
DUA-18-T32B	24.54	24.84						
DUA-18-T32C	24.84	25.05						

Mag: magnetite; Pcl: pyrochlore; Pvr: perovskite; Pyr: pyrite; Pho: pyrrhotite; Sph: sphalerite.

Table 9: Tailings mineralogy by SEM. Minor carbonate and sulfate minerals. Shaded samples are in the soil underlying the impoundment. Common (X); present (x); not detected (-)

Sample No.	Depth from (m)	Depth to (m)	Dol	Str	Rds	Par	Anc	Brt
DUA-18-T1	0.00	0.61	x	-	-	-	-	-
DUA-18-T2	0.76	1.37	x	-	-	-	-	x
DUA-18-T3	1.52	2.13	-	-	x	x	-	-
DUA-18-T4A	2.29	2.44	-	x	-	-	-	-
DUA-18-T4B	2.44	2.59	x	-	-	x	-	-
DUA-18-T4C	2.59	2.90	-	x	-	x	-	x
DUA-18-T5	3.05	3.66	x	-	-	x	x	x
DUA-18-T6A	3.81	4.27	-	-	-	x	-	x
DUA-18-T6B	4.27	4.42	-	-	-	-	-	x
DUA-18-T7	4.88	5.18	x	-	-	x	-	x
DUA-18-T8A	5.64	5.79	x	-	-	x	-	x
DUA-18-T8B	5.79	5.94	x	-	-	-	-	-
DUA-18-T9	6.40	6.71	-	-	-	-	-	X
DUA-18-T10	7.16	7.47	x	-	-	-	-	x
DUA-18-T11	7.92	8.23	X	-	-	-	-	x
DUA-18-T12	8.69	8.99	-	-	-	-	-	x
DUA-18-T13A	9.14	9.45	-	x	-	-	-	x
DUA-18-T13B	9.45	9.75	x	X	-	-	-	X
DUA-18-T14	10.21	10.52	x	x	-	x	-	x
DUA-18-T15A	10.67	10.97	X	-	-	x	-	X
DUA-18-T15B	10.97	11.28	X	x	-	x	-	X
DUA-18-T16	11.73	12.04	-	x	x	-	-	x
DUA-18-T17	12.34	12.65	x	x	-	-	-	x
DUA-18-T18	13.11	13.41	x	x	x	-	-	x
DUA-18-T19	14.02	14.33	X	x	x	x	-	X
DUA-18-T20	14.63	14.94	X	x	x	x	-	X
DUA-18-T21	15.54	15.85	X	-	-	-	-	x
DUA-18-T22A/B	16.15	16.61	x	x	-	x	x	x
DUA-18-T23A/B	16.76	17.37	X	x	x	x	-	X
DUA-18-T24	17.53	18.14	X	x	x	-	-	x
DUA-18-T25	18.44	18.75	-	x	-	-	-	x
DUA-18-T26	19.35	19.66	-	x	-	-	-	x
DUA-18-T27	20.12	20.42	-	-	-	-	-	x
DUA-18-T28	20.57	21.18	X	x	x	-	-	X
DUA-18-T29	21.34	21.95	X	x	x	-	-	x
DUA-18-T30	22.25	22.56	x	x	-	-	-	-
DUA-18-T31	22.86	23.47	x	-	-	-	x	x
DUA-18-T32A	24.38	24.54						
DUA-18-T32B	24.54	24.84						
DUA-18-T32C	24.84	25.05						

Dol: dolomite; Str: strontianite; Rds: rhodochrosite; Par: parisite; Anc: ancylite; Brt: barite.

Table 10: Tailings mineralogy by SEM. Minor silicate minerals. Shaded samples are in the soil underlying the impoundment. Common (X); present (x); not detected (-)

Sample No.	Depth from (m)	Depth to (m)	Nep	Mtc	Amp	Cpx	Sme	Kln	Zeo
DUA-18-T1	0.00	0.61	-	-	x	x	-	x	x
DUA-18-T2	0.76	1.37	-	-	x	X	-	x	-
DUA-18-T3	1.52	2.13	-	-	x	X	-	-	x
DUA-18-T4A	2.29	2.44	x	-	-	X	-	-	x
DUA-18-T4B	2.44	2.59	X	-	-	X	-	-	x
DUA-18-T4C	2.59	2.90	-	-	-	x	-	-	-
DUA-18-T5	3.05	3.66	-	-	-	x	x	x	-
DUA-18-T6A	3.81	4.27	x	-	x	-	x	-	-
DUA-18-T6B	4.27	4.42	-	-	x	-	-	-	x
DUA-18-T7	4.88	5.18	x	-	x	-	x	-	-
DUA-18-T8A	5.64	5.79	x	-	x	X	x	x	-
DUA-18-T8B	5.79	5.94	x	-	x	x	x	x	x
DUA-18-T9	6.40	6.71	-	-	x	x	-	-	x
DUA-18-T10	7.16	7.47	x	x	x	x	x	-	x
DUA-18-T11	7.92	8.23	-	x	X	x	-	-	X
DUA-18-T12	8.69	8.99	X	-	x	X	-	x	X
DUA-18-T13A	9.14	9.45	x	x	-	x	-	-	-
DUA-18-T13B	9.45	9.75	-	-	x	-	-	x	x
DUA-18-T14	10.21	10.52	-	-	x	x	-	x	x
DUA-18-T15A	10.67	10.97	x	-	x	x	-	-	X
DUA-18-T15B	10.97	11.28	-	-	x	x	-	x	x
DUA-18-T16	11.73	12.04	-	-	-	X	-	-	x
DUA-18-T17	12.34	12.65	x	-	-	X	-	x	X
DUA-18-T18	13.11	13.41	x	-	-	X	-	x	X
DUA-18-T19	14.02	14.33	-	-	x	X	-	-	x
DUA-18-T20	14.63	14.94	x	x	x	-	-	x	x
DUA-18-T21	15.54	15.85	-	x	X	X	-	-	X
DUA-18-T22A/B	16.15	16.61	-	x	X	X	-	-	x
DUA-18-T23A/B	16.76	17.37	x	-	x	x	-	-	-
DUA-18-T24	17.53	18.14	x	-	-	X	-	-	X
DUA-18-T25	18.44	18.75	-	-	x	X	-	-	X
DUA-18-T26	19.35	19.66	-	-	x	X	-	-	X
DUA-18-T27	20.12	20.42	x	-	x	X	-	-	x
DUA-18-T28	20.57	21.18	-	-	-	X	-	-	-
DUA-18-T29	21.34	21.95	-	-	-	X	-	-	x
DUA-18-T30	22.25	22.56	x	-	-	X	-	-	X
DUA-18-T31	22.86	23.47	-	x	-	X	-	-	X
DUA-18-T32A	24.38	24.54							
DUA-18-T32B	24.54	24.84							
DUA-18-T32C	24.84	25.05							

Nep: nepheline; Mtc: monticellite; Amp: amphibole (mainly richterite); Cpx: clinopyroxene (including aegirine and diopside); Sme: smectite; Kln: kaolinite; Zeo : zeolite (mainly natrolite and analcime)

4.2.3 Energy Dispersive X-Ray Spectroscopy and Electron Probe Microanalysis

Pyrochlore and apatite are the two main host phases for critical minerals in the SLC tailings. Pyrochlore is a host for Nb and also for REEs and Zr. Apatite is a host for P and REEs. This section reviews the compositions of pyrochlore and apatite, as determined by Energy Dispersive X-ray Spectroscopy (EDS) and Electron Probe Microanalysis (EPMA).

Pyrochlore

Qualitative SEM-EDS analyses (not shown) indicate that pyrochlore grains tend to be Ce-rich with minor Nd. Some grains show the presence of major to minor U. Thorium, Zr and Ta were also detectable in some grains. Any Si present may reflect the presence of silicates as some grains may not be isolated.

Electron probe microanalysis (EPMA) was used to obtain quantitative measurements of pyrochlore grain compositions from 11 samples representing different depth horizons within the tailings impoundment (Figure 11). All results are reported as wt.% oxide. Grain concentrations of Nb_2O_5 within a sample vary by less than an order of magnitude (Figure 11a). The variability of other elements substituting in the pyrochlore "B" site (Ti, Ta, Zr) is much greater and exceeds two orders of magnitude (Figure 11b, c, d). Pyrochlore grains fall into two groups with respect to their ZrO_2 content. Although most grains have a ZrO_2 content less than 10 wt.%, a small number have contents greater than 30 %. The UO_2 and ThO_2 concentrations in pyrochlore grains vary over four orders of magnitude (Figure 11e, f), reaching 15.9% and 19.1%, respectively. Concentrations of REEs, which also substitute in the pyrochlore "A" site, are less variable (Figure 11g, h, i). Maximum concentrations of Ce_2O_3, Nd_2O_3, and Dy_2O_3, can exceed 10%, 3%, and 1%, respectively. Mean concentrations of the main pyrochlore grain constituents do not show any discernable trend with sample depth (Table 11).

In Table 12, the mean EPMA composition of all pyrochlore grains is compared to the mean EPMA composition of pyrochlore grains from an archived sample of concentrate (PNA15-11). These compositions, in turn, are compared with results of a chemical analysis of SLC pyrochlore concentrate reported by Gold et al. (1967). While there is a general qualitative agreement between the concentrate compositions, there are some notable differences with the mean composition of pyrochlore grains from tailings samples. The mean Nb_2O_5 content of pyrochlore in the tailings (52.9%) is lower than the mean concentrations in concentrate grains (55.9%) and in concentrate (60%). On the other hand, the mean UO_2 and ThO_2 concentrations in pyrochlore from tailings samples (0.77% and 0.74%, respectively) are much higher than values measured in concentrate. However, this may be simply a reflection of the much greater blending of pyrochlore that occurs during the concentration process.

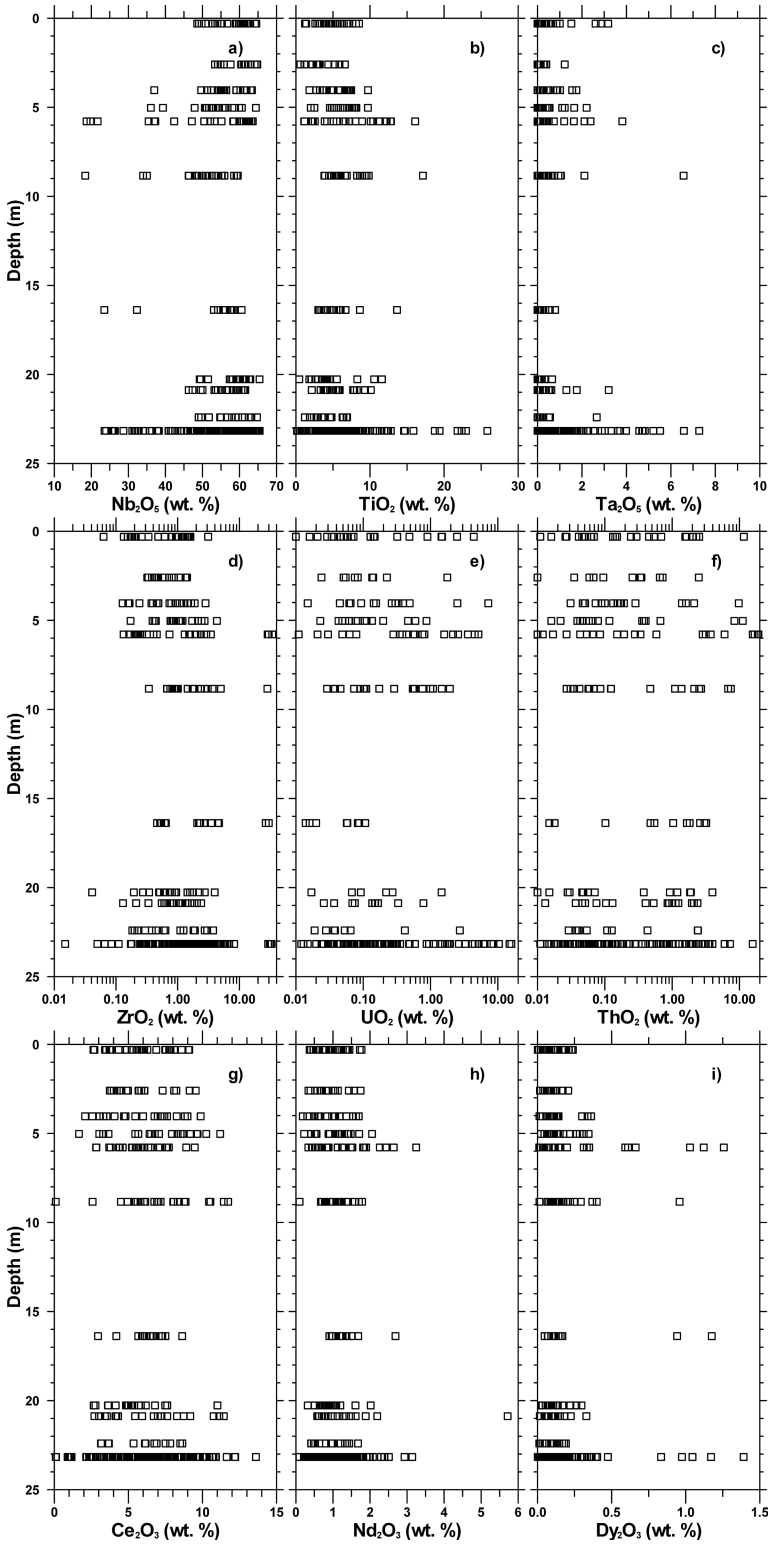

Figure 11: Depth profiles in the GSC borehole of pyrochlore grain compositions from microprobe analyses.

Table 11: Mean pyrochlore grain (> 63 μm) compositions (wt. %) from EPMA analyses of selected tailings samples.

	DUA18-T1	DUA18-T4	DUA18-T6A	DUA18-T7	DUA18-T8	DUA18-T12
Depth (m)	0.3	2.6	4.0	5.0	5.8	8.8
	n=31	n=18	n=22	n=20	n=25	n=23
Nb_2O_5	57.96	60.08	56.23	53.35	49.25	49.61
Ta_2O_5	0.52	0.15	0.38	0.45	0.70	0.72
TiO_2	4.64	3.39	5.43	6.31	6.78	6.99
ZrO_2	0.83	0.69	0.92	1.25	4.58	2.83
FeO	1.32	1.62	1.25	1.28	2.57	1.76
MnO	0.23	0.25	0.28	0.32	0.85	0.45
CaO	15.97	16.13	15.63	15.17	11.64	14.59
Na_2O	4.42	4.53	4.27	3.74	2.55	2.91
SiO_2	0.12	0.01	0.32	1.09	0.86	1.41
WO_3	<0.01	<0.01	<0.01	<0.01	<0.01	<0.01
UO_2	0.40	0.14	0.55	0.15	0.98	0.39
ThO_2	0.80	0.28	0.75	1.10	3.51	1.15
Y_2O_3	0.10	0.12	0.09	0.12	0.15	0.15
La_2O_3	1.09	1.02	1.02	1.07	1.09	0.90
Ce_2O_3	5.85	5.91	5.75	7.08	5.72	6.99
Pr_2O_3	0.32	0.30	0.29	0.33	0.32	0.31
Nd_2O_3	0.93	0.89	0.89	1.09	1.27	1.07
Sm_2O_3	0.17	0.15	0.15	0.19	0.24	0.19
Eu_2O_3	0.03	0.03	0.02	0.05	0.06	0.05
Gd_2O_3	0.07	0.10	0.12	0.14	0.12	0.13
Tb_2O_3	0.01	0.01	0.01	0.01	0.01	0.01
Dy_2O_3	0.10	0.10	0.12	0.15	0.31	0.20
Ho_2O_3	0.02	0.02	0.01	0.02	0.02	0.01
Er_2O_3	0.01	0.01	0.01	0.01	0.02	0.02
Tm_2O_3	0.01	0.01	0.01	0.01	0.02	0.02
Yb_2O_3	0.03	0.03	0.02	0.02	0.03	0.03
Lu_2O_3	0.01	0.01	0.01	0.01	0.01	<0.01
∑REEO	8.65	8.57	8.44	10.17	9.22	9.34
F	3.55	3.64	3.44	3.13	2.07	2.53
Total	98.02	98.09	96.54	96.33	94.84	94.39

Table 11 (continued): Mean pyrochlore grain (> 63 μm) compositions (wt. %) from EPMA analyses of selected tailings samples.

	DUA18-T22	DUA18-T27	DUA18-T28	DUA18-T30	DUA18-T31	DUA18-T31*
Depth (m)	16.4	20.3	20.9	22.4	23.1	23.1
	n=15	n=20	n=20	n=15	n=125	n=34
Nb_2O_5	52.72	58.91	55.98	58.05	51.64	54.72
Ta_2O_5	0.19	0.08	0.50	0.30	0.87	0.85
TiO_2	5.50	4.34	5.54	4.40	6.50	5.42
ZrO_2	5.66	1.09	1.03	1.23	3.03	1.53
FeO	2.05	1.42	1.36	1.63	1.88	1.26
MnO	0.63	0.25	0.23	0.23	0.39	0.28
CaO	15.77	15.63	16.47	16.13	15.64	14.75
Na_2O	3.74	4.61	4.58	4.48	3.80	4.29
SiO_2	<0.01	0.13	<0.01	0.25	0.79	0.57
WO_3	<0.01	<0.01	<0.01	<0.01	0.01	<0.01
UO_2	0.03	0.11	0.10	0.23	0.67	1.01
ThO_2	0.96	0.53	0.69	0.38	0.46	0.84
Y_2O_3	0.16	0.12	0.12	0.13	0.13	0.12
La_2O_3	1.06	0.90	1.11	1.08	1.09	1.16
Ce_2O_3	6.34	5.43	6.45	5.93	6.22	6.50
Pr_2O_3	0.39	0.30	0.40	0.31	0.34	0.37
Nd_2O_3	1.35	0.90	1.29	0.96	1.06	1.12
Sm_2O_3	0.25	0.16	0.22	0.15	0.19	0.20
Eu_2O_3	0.06	0.02	0.04	0.03	0.04	0.03
Gd_2O_3	0.12	0.11	0.13	0.10	0.12	0.13
Tb_2O_3	0.01	0.01	0.01	0.01	0.01	0.01
Dy_2O_3	0.24	0.11	0.11	0.10	0.16	0.12
Ho_2O_3	0.02	0.02	0.03	0.02	0.02	0.01
Er_2O_3	0.01	0.01	0.01	0.01	0.01	0.01
Tm_2O_3	0.01	0.01	0.01	0.01	0.02	0.02
Yb_2O_3	0.04	0.03	0.04	0.03	0.04	0.04
Lu_2O_3	<0.01	0.01	0.01	<0.01	0.01	0.01
∑REEO	9.92	8.01	9.86	8.74	9.34	9.73
F	2.91	3.77	3.82	3.66	2.83	3.39
Total	99.04	97.41	98.70	98.30	96.79	97.36

* grains > 2 μm

Table 12: Mean pyrochlore grain compositions (wt. %) from EPMA analyses of all tailings samples and comparison with the mean composition of grains from an archived sample of pyrochlore concentrate and the average pyrochlore concentrate composition from Gold et al. (1967).

	All grains	PNA15-11 Conc.	Conc.*
	n=429	n=20	-
Nb_2O_5	52.90	55.91	60.00
Ta_2O_5	1.00	0.41	0.50
TiO_2	5.82	3.79	4.30
ZrO_2	2.41	1.89	1.00
FeO	1.69	1.75	2.43
MnO	0.40	0.34	0.37
CaO	15.54	15.97	15.09
Na_2O	3.77	4.19	3.50
SiO_2	0.51	0.21	n.a.
WO_3	0.01	< 0.01	n.a.
UO_2	0.77	0.11	0.10
ThO_2	0.74	0.06	0.23
Y_2O_3	0.13	0.15	0.12
La_2O_3	1.07	1.10	0.70
Ce_2O_3	6.48	7.26	3.00
Pr_2O_3	0.34	0.33	n.a
Nd_2O_3	1.10	1.08	n.a.
Sm_2O_3	0.20	0.20	n.a.
Eu_2O_3	0.04	0.05	n.a.
Gd_2O_3	0.12	0.15	0.20
Tb_2O_3	0.01	0.02	n.a.
Dy_2O_3	0.17	0.15	n.a.
Ho_2O_3	0.02	0.02	n.a.
Er_2O_3	0.01	0.01	n.a.
Tm_2O_3	0.02	0.01	n.a.
Yb_2O_3	0.03	0.03	n.a.
Lu_2O_3	0.01	0.00	n.a.
∑REEO	9.62	10.42	n.a.
F	3.02	3.44	3.69
Total	97.08	97.19	n.a.

* sample 9 from table IV of Gold et al. (1967)

Apatite

Qualitative SEM-EDS analyses (not shown) indicate that apatite grains tend to be La and Ce-rich with minor Nd and variable F. Some grains show the presence of aluminum and strontium. Measurements by EPMA provide greater detail on the variability of apatite grain compositions in tailings samples from different depths (Figure 12). The variability of the main apatite constituents (CaO, P_2O_5, F) is relatively low, particularly when compared to the variability exhibited by pyrochlore grain compositions (Figure 11). Rare earth element concentrations in apatite grains are lower than in pyrochlore grains, and are much less variable (Figure 12, Table 13). As with pyrochlore grain compositions, there is no apparent depth trend in apatite compositions (Table 13).

Table 13: Mean apatite grain (> 63 μm) compositions (in wt. %) from EPMA analyses of selected tailings samples.

	DUA18-T6A	DUA18-T7	DUA18-T12	DUA18-T27	DUA18-T28	DUA18-T31
Depth (m)	4.0	5.0	8.8	20.3	20.9	23.1
	n=20	n=20	n=20	n=20	n=21	n=20
P_2O_5	38.86	38.93	38.67	38.96	39.23	38.50
CaO	51.82	52.02	52.05	51.98	52.14	51.89
SrO	1.18	0.98	1.06	1.14	1.17	0.98
Na_2O	0.06	0.06	0.01	0.02	0.04	0.01
FeO	0.05	0.06	0.05	0.02	0.04	0.01
MnO	0.05	0.06	0.05	0.07	0.07	0.05
F	3.28	3.31	3.29	3.30	3.35	3.22
Cl	0.01	0.01	0.01	0.00	0.01	0.00
SO_3	0.12	0.16	0.18	0.11	0.14	0.19
Y_2O_3	0.04	0.06	0.05	0.04	0.05	0.07
La_2O_3	0.82	0.76	0.69	0.78	0.73	0.86
Ce_2O_3	1.50	1.31	1.11	1.36	1.24	1.50
Pr_2O_3	0.14	0.15	0.11	0.14	0.11	0.14
Nd_2O_3	0.49	0.45	0.36	0.44	0.39	0.48
Sm_2O_3	0.08	0.06	0.07	0.06	0.06	0.08
Eu_2O_3	0.02	0.02	0.01	0.02	0.01	0.02
Gd_2O_3	0.03	0.04	0.04	0.05	0.05	0.06
Tb_2O_3	0.00	0.00	0.01	0.01	0.01	0.01
Dy_2O_3	0.03	0.04	0.03	0.04	0.03	0.03
Ho_2O_3	0.01	0.01	0.01	0.01	0.01	0.01
Er_2O_3	0.01	0.00	0.00	0.01	0.01	0.01
Tm_2O_3	0.01	0.01	0.01	0.01	0.01	0.01
Yb_2O_3	0.01	0.01	0.01	0.01	0.02	0.02
Lu_2O_3	0.01	0.01	0.01	0.00	0.00	0.02
∑REEO	3.19	2.89	2.47	2.94	2.69	3.25
Total	98.49	98.32	97.68	98.35	98.54	98.31

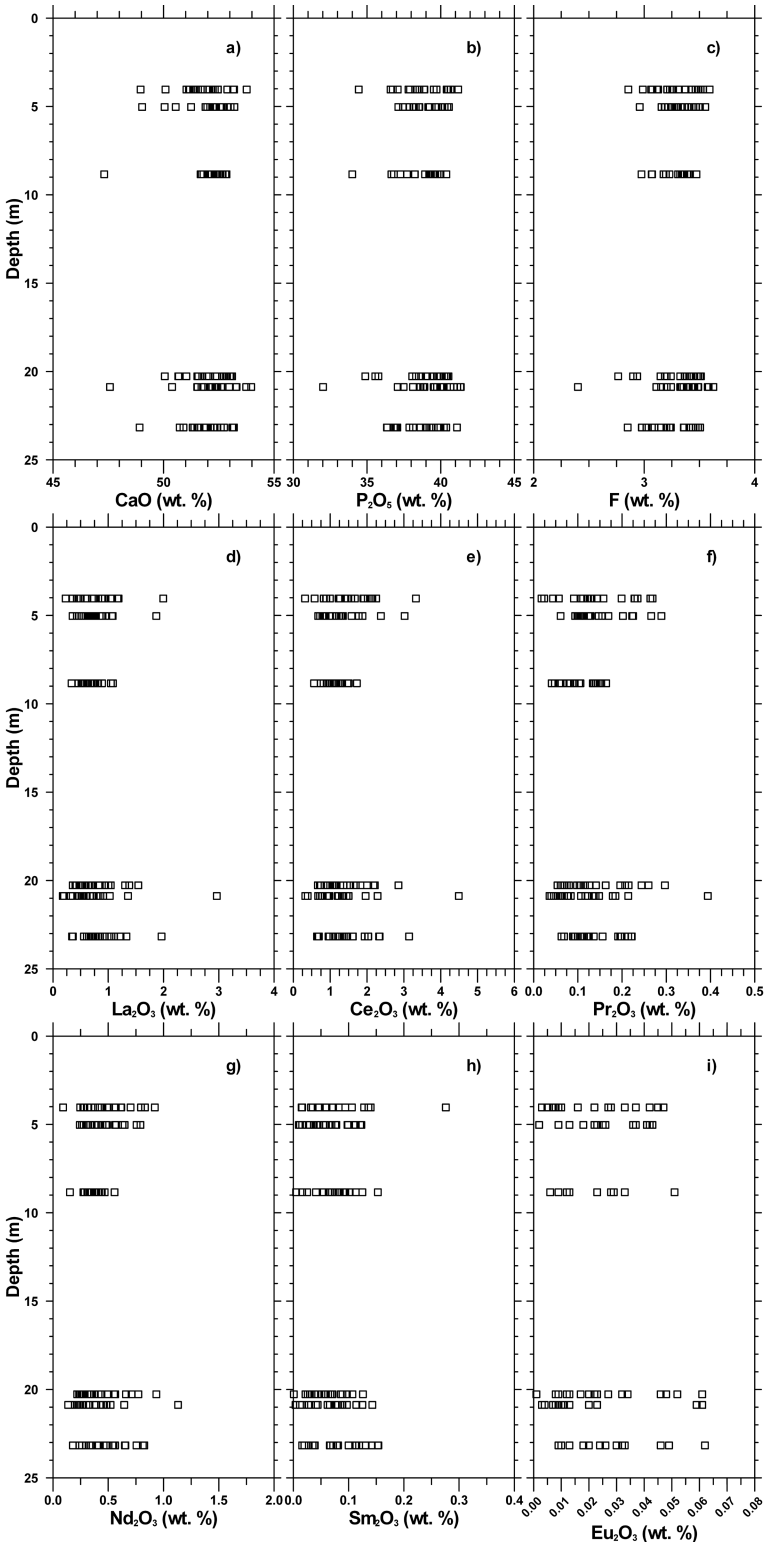

Figure 12: Depth profiles in the GSC borehole of apatite grain compositions from microprobe analyses.

4.3 Tailings Geochemistry

Detailed depth profiles of tailings bulk geochemistry from the GSC borehole reflect the temporal evolution of milling and tailings disposal practices over the mine life. They also provide a measure of the amounts and spatial distribution of any unrecovered mineral resource.

The depth profile for CaO (Figure 13) reflects the fairly uniform calcite content of tailings shown in Figure 10a. Similarly, the MgO, SiO_2, and K_2O profiles (Figure 13) reflect the biotite content shown in Figure 10b. All four profiles clearly reveal the sharp geochemical contrast between carbonatite tailings and the underlying soil layer composed mainly of silicate minerals likely derived from the surrounding fenitized gneiss.

Depth profiles of Fe_2O_3 (total Fe), MnO, TiO_2, and V (Figure 14) highlight the vertical distribution of magnetite-rich horizons notably from 20 to 22 m below ground surface and at the top of the soil layer (Table 5). Titanium, Mn, and V are common substitutions in magnetite. Iron contained in biotite likely accounts for the more uniform background Fe_2O_3 concentrations in the tailings.

Depth profiles of P_2O_5, F, Y, and total REE reveal the presence of several fluorapatite-rich layers, at 9 m, 20-22 m, and at 23-24 m (Figure 15). While F concentrations generally follow those of P_2O_5, there are discrete F-rich horizons that do not fit this pattern. Total REE concentrations, on the other hand, follow P_2O_5 values more closely and sometimes reach 3.25 wt.% (Table 13).

Depth profiles of Nb, Th, U, and Zr characterize variations in pyrochlore composition and reflect the efficiency of the milling process (Figure 16). Coincident spikes in Nb and one or more of these elements indicate layers containing significant unrecovered pyrochlore. The most important of these layers, where Nb reaches ore-grade concentrations, is between 20 and 22 m below ground surface. Uranium and Th concentrations in the layer reach 80 and 175 ppm, respectively. Higher in the tailings sequence, Nb concentrations are much lower and more uniform. This suggests a stabilization of ore processing with improved pyrochlore recovery. Background Nb concentrations reflect unrecovered pyrochlore and possibly minor Nb hosted in perovskite (latrappite).

Total S and Zn exhibit fairly uniform depth profiles except for pronounced coincident spikes in the sandy basal layer suggesting the presence of sphalerite (Figure 17) in addition to the pyrite noted above. Depth profiles of Pb and Mo also suggest the presence of sulfide-rich horizons (Figure 17). From these and preceding geochemical depth profiles, it appears that coarse and/or dense tailings containing abundant magnetite, apatite, sulphides, and unrecovered pyrochlore were deposited early in the mine life as the milling process was being adjusted.

Summary statistics for selected trace element concentrations in the tailings are provided in Table 14. For elements subject to Quebec environmental standards for the protection of soils and the remediation of contaminated sites (MDDELCC, 2016), the table also lists the percentage of samples exceeding the regulatory threshold. All samples exceeded level “A” background criteria for Mn, Mo, Zn, and Cd.

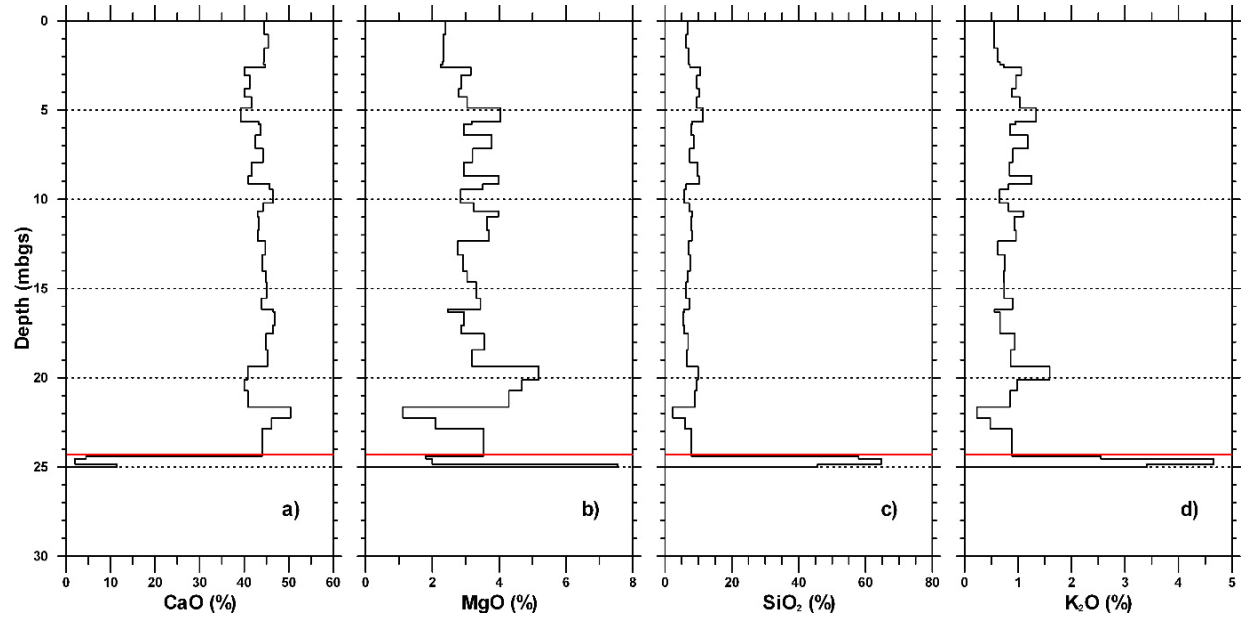

Figure 13: Downhole profiles of tailings chemistry: a) CaO; b) MgO; c) SiO_2; and d) K_2O.

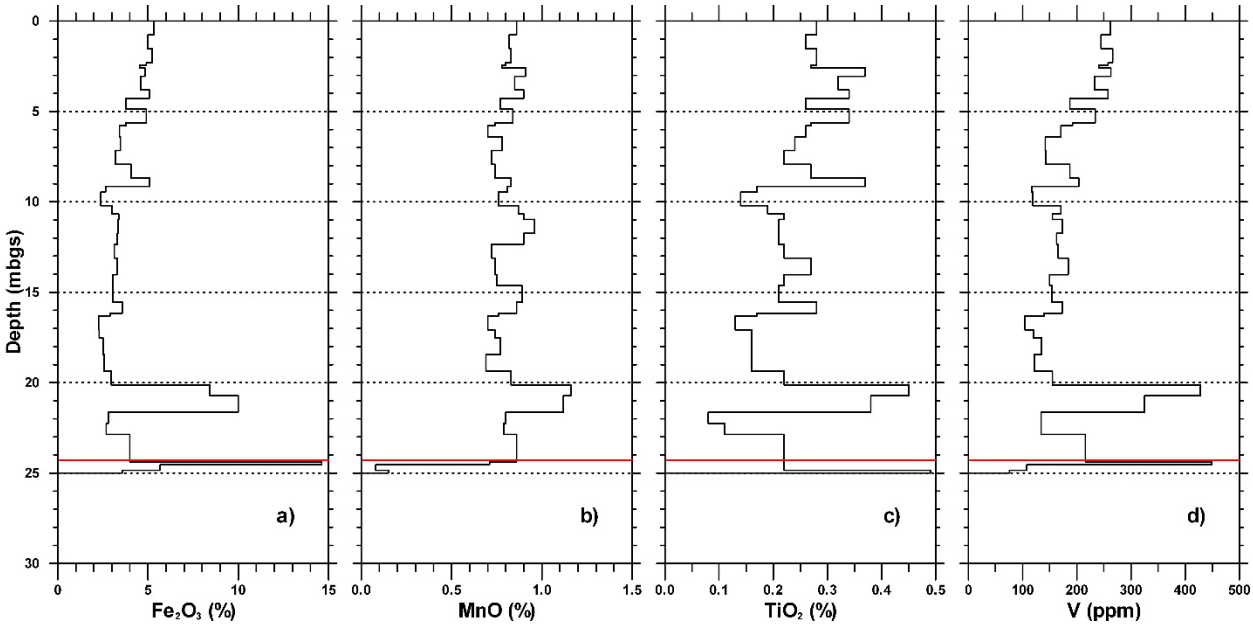

Figure 14: Downhole profiles of tailings chemistry: a) Fe_2O_3; b) MnO; c) TiO_2; and d) V.

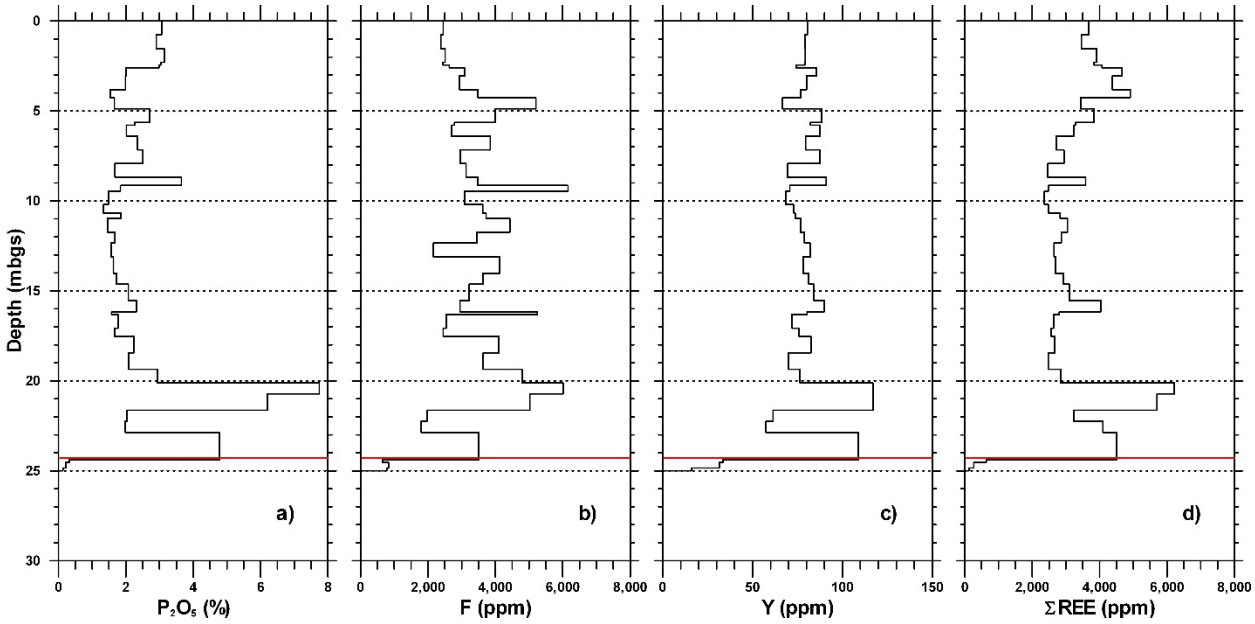

Figure 15: Downhole profiles of tailings chemistry: a) P_2O_5; b) F; c) Y; and d) Σ REE.

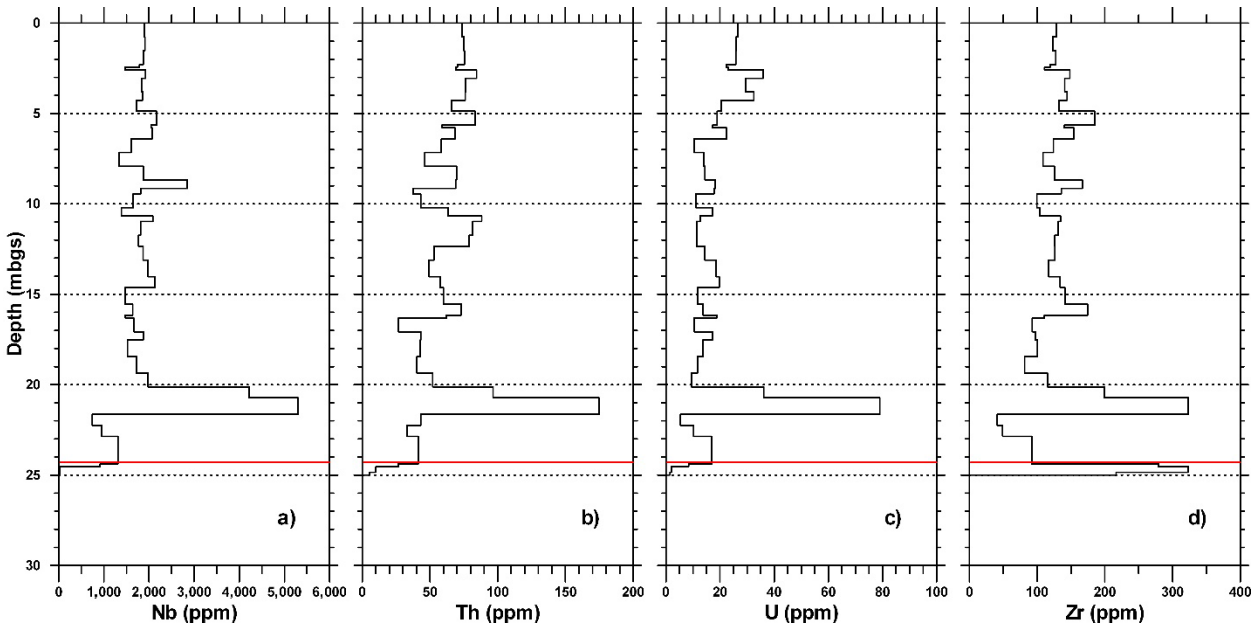

Figure 16: Downhole profiles of tailings chemistry: a) Nb; b) Th; c) U; and d) Zr.

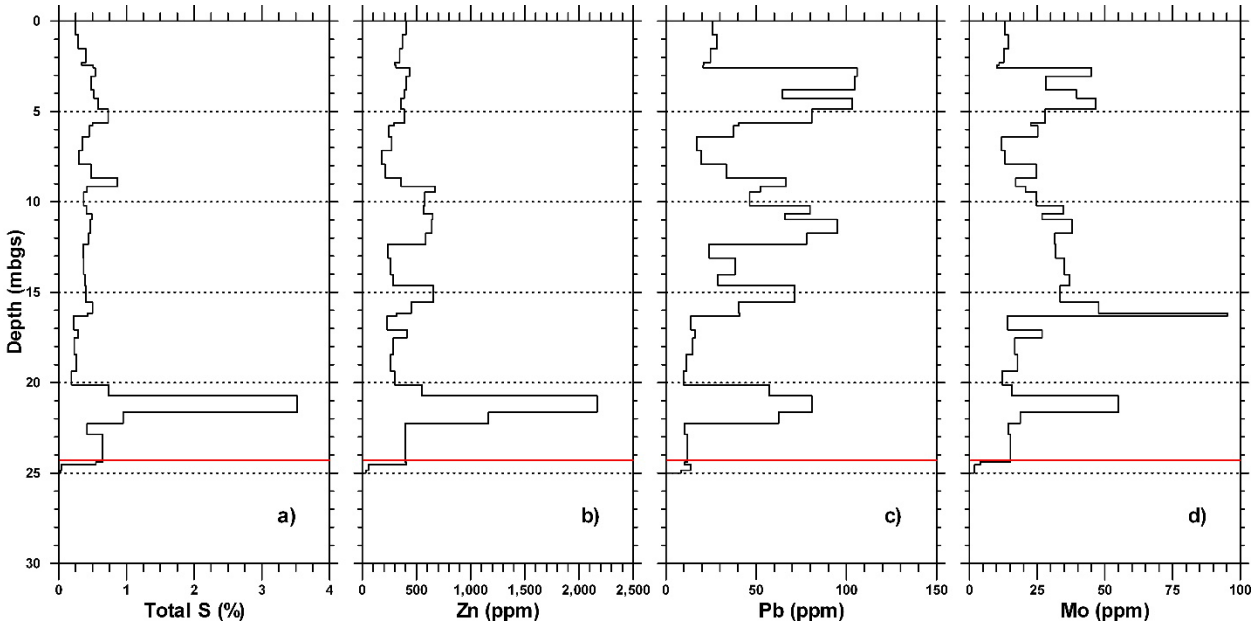

Figure 17: Downhole profiles of tailings chemistry: a) Total S; b) Zn; c) Pb; and d) Mo.

Table 14: Tailings bulk chemistry: Summary statistics for concentrations of selected trace elements with MDDELCC regulatory criteria for the protection of soils and the remediation of contaminated sites, and their exceedance percentages.

	n	Min. (ppm)	Max. (ppm)	Median (ppm)	Mean (ppm)	Std. (ppm)	Crit.* (ppm)	Exceed. (%)
Ag	38	0.1	1.4	0.3	0.4	0.2	2	0
As	38	1.9	17.6	3.6	4.1	2.5	6	5
Be	38	1.0	6.0	2.0	2.5	1.4	-	-
Cd	38	1.5	15.7	3.7	4.3	2.5	1.5	100
Cr	38	13.7	34.2	20.5	20.5	6.8	100	0
Co	38	2.0	14.8	4.3	4.9	2.4	25	0
Cu	38	4.9	41.6	8.5	10.6	6.1	50	0
Hg	38	0.01	0.01	0.01	0.01	0.00	0.2	0
Mn	38	5,344	8,984	6,234	6,369	784	1,000	100
Mo	38	10	95	25	27	16	2	100
Ni	38	0.1	7.4	2.3	2.2	1.4	50	0
Pb	38	9.7	105.9	39.3	45.9	29.6	50	39
Se	38	0.5	2.7	0.5	0.6	0.4	1	8
Th	38	27	175	64	65	30	-	-
U	38	5	79	17	20	12	-	-
Zn	38	181	2,167	378	456	339	140	100

* MDDELCC (2016) criteria for soils and contaminated sites level “A” for background.

5. DISCUSSION AND CONCLUSIONS

5.1 Niobium

According to historical production figures from the SLC mine (Niocan, 2010), the average grade of milled ore was 0.46 wt. % Nb_2O_5 and the recovery efficiency of the mill was about 68 % (Table 1). The average grade of the tailings then should be approximately 0.15 wt.% Nb_2O_5. This estimate is considerably lower than the average grade of tailings based on GSC borehole samples, which is 0.27 wt.% Nb_2O_5 (Table 15). However, the latter estimate is influenced by the high Nb grades in the layer of dense, coarse-grained material near the base of the tailings (Figure 16). The lateral extent of this high-grade layer is unknown. Because of its highly variable composition, the density of pyrochlore is variable also. Carbonneau and Caron (1965) assume that 0.5 wt. % Nb_2O_5 is equivalent to 1 wt. % pyrochlore. Thus, the pyrochlore content of the tailings is estimated at 0.3 wt. % based on historical production figures or 0.54 wt. % based on the GSC borehole samples.

5.2 Phosphorus

Based on bulk XRD analyses, the average apatite content of the tailings is 5 wt.% (Table 4). Based on bulk geochemistry, the mean P_2O_5 content of the tailings is 2.46 wt.% (Table 15). Assuming an apatite molecular weight of 504.32 g/mol, the corresponding apatite content of the tailings is approximately 5.8%. Given the variability of apatite compositions (Table 13), the agreement between these two estimates is reasonable. However, both estimates are based on tailings samples from the GSC borehole and therefore are influenced by the high apatite content of the dense, coarse-grained layer near the base of the impoundment (Figure 15).

5.3 Rare Earth Elements

Rare earth elements in the SLC tailings are mostly concentrated in pyrochlore and apatite although they are also hosted in calcite (Eby, 1975; Hornig-Kjarsgaard, 1998). If the pyrochlore content of the tailings varies between 0.3 and 0.54 wt.% and the total REE oxide (ΣREEO) content of pyrochlore varies between 9.62 and 10.42 wt.% (Table 12), the tailings contain between 0.029 and 0.056 wt.% ΣREEO hosted in pyrochlore. Similarly, if the apatite content of tailings varies between 5 and 5.8 wt.% and the ΣREEO content of apatite varies between 2.47 and 3.25 wt.% (Table 13), the tailings contain between 0.12 and 0.19 wt. % ΣREEO hosted in apatite. These values can be compared with the mean ΣREEO content of bulk tailings of 0.4 wt.% (Table 15). Thus, a significant portion of the REE inventory within the tailings is hosted by calcite.

Chondrite normalized REE concentrations (Figure 18) show that both pyrochlore and apatite are enriched in light REE (LREE) relative to heavy REE (HREE) and that pyrochlore is more enriched in REEs than apatite. The overall distribution patterns are similar with an apparent plateau in HREE (albeit erratic due to the number of samples with below detection limit concentrations) and a general increase in concentrations from Dy to La. The distribution pattern for pyrochlore exhibits a distinct Ce anomaly, however. Similar observations were made by Hornig-Kjarsgaard (1998) in apatite and pyrochlore mineral separate samples from the Oka Carbonatite Complex.

Table 15: Tailings bulk chemistry: Summary statistics for selected tailings constituents.

	n	Min. (%)	Max. (%)	Median (%)	Mean (%)	Std. (%)
F	38	0.18	0.61	0.33	0.35	0.11
Fe_2O_3	38	2.26	9.99	3.40	3.92	1.57
Nb_2O_5	38	0.11	0.76	0.26	0.27	0.11
P_2O_5	38	1.33	7.74	2.02	2.46	1.30
S (total)	38	0.19	3.52	0.42	0.53	0.53
SiO_2	38	2.35	11.39	7.39	7.64	1.76
∑REEO	38	0.28	0.73	0.37	0.40	0.10

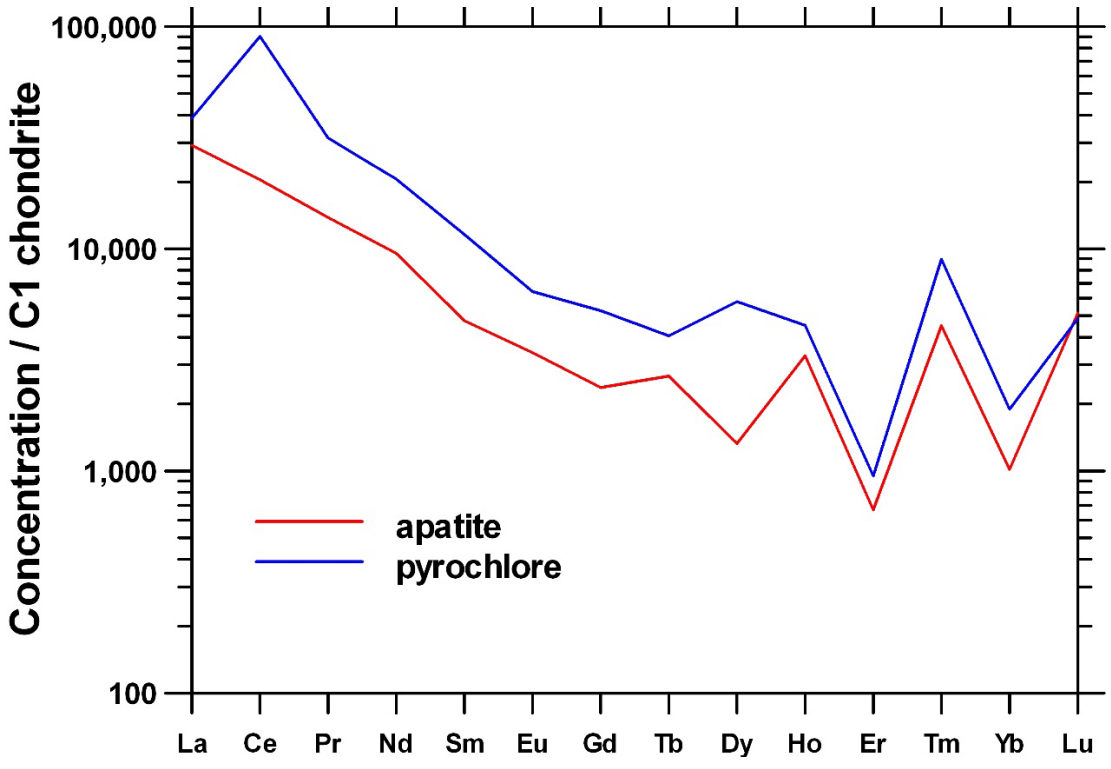

Figure 18: REE distribution patterns in apatite and pyrochlore based on average grain concentrations determined by EPMA. REE concentrations are normalized by C1 chondrite abundances from McDonough and Sun (1995).

5.4 Deleterious Substances

The Nb product for market is ferroniobium alloy, which is obtained through the aluminothermic reduction of pyrochlore concentrate (Desbarats et al., 2020b; Desbarats et al., 2024). Essentially all the trace elements contained in the pyrochlore partition into the slag residue resulting from the conversion process. This includes all the REEs and Zr, as well as all the U and Th. However, U and Th concentrations in the slag are greatly enhanced compared to the ore. As a result, the slag represents a technologically enhanced naturally occurring radioactive material (TENORM) requiring special environmental management. Slag at the SLC site was disposed of on surface, outside the tailings impoundment area.

The SiO_2 concentrations reflect the ferromagnesian silicate content of the tailings (Table 15), which is mainly in the form of fine-grained biotite and chlorite, as shown in Figures 8 and 10, and Table 5. These minerals were problematic for milling operations (Carbonneau and Caron, 1965).

Concentrations of total S, mainly as sulfide, vary between 0.19 and 3.52 wt. % with a mean value of 0.53 wt. % (Table 15). Although these concentrations are relatively high, the overwhelming abundance of calcite in the tailings provides ample acid neutralization potential and tailings seepage waters were found to have a mean pH of 7.8 (Desbarats et al., 2020a; 2022).

5.5 Resource Estimation Considerations

Different waste streams from the mill (section 2.4), varying tailings disposal schemes over the mine life (section 2.5), and textural and density segregation processes in waste slurries have resulted in significant mineralogical and geochemical heterogeneity within the tailings impoundment (sections 4.1-4.3). In essence, the tailings can be viewed as an anthropogenic sedimentary mineral deposit. Estimation of their resource potential similarly requires systematic drilling and sophisticated data analysis (Mulenshi et al., 2021; Blannin et al., 2023).

REFERENCES

Araya, N., Ramirez, Y., Kraslawski, A., Cisternas, L.A., 2021. Feasibility of reprocessing mine tailings to obtain critical raw materials using real options analysis. Jour. Environmental Management, 284, 112060; https://doi.org/10.1016/j.jenvman.2021.112060

Berger, V. I., Singer, D. A., and Orris, G.J., 2009. Carbonatites of the world, explored deposits of Nb and REE- Database and grade and tonnage models; U. S. Geological Survey Open-File Report 2009-1139, 17 p. and database.

Blannin, R., Frenzel, M., Tolosana-Delgado, R., Büttner, P., and Gutzmer, J., 2023. 3D geostatistical modelling of a tailings storage facility: Resource potential and environmental implications. Ore Geology Review, 154, 105337; https://doi.org/10.1016/j.oregeorev.2023.105337

Carbonneau, C., and Caron, J.C., 1965. The production of pyrochlore concentrates at St. Lawrence Columbium and Metals Corp.; Trans. Can. Inst. Min., 68, 71-79.

Chen, W., and Simonetti, A., 2013. In-situ determination of major and trace elements in calcite and apatite, and U-Pb ages of apatite from the Oka carbonatite complex: Insights into a complex crystallization history; Chemical Geology, 353, 151-172; https://doi:10.1016/j.chemgeo.2012.04.022

Chen, W., and Simonetti, A., 2014. Evidence for the Multi-Stage Petrogenetic History of the Oka Carbonatite Complex (Quebec, Canada) as Recorded by Perovskite and Apatite; Minerals, 4, 437-476; https://doi:10.3390/min4020437.

Desbarats, A.J., Percival, J.B., Pelchat, P., Sekerka, J., Bilot, I., Girard, I., and Gammon, P., 2020a. Geoenvironmental characterization of carbonatite tailings, Saint Lawrence Columbium Minea, Oka, Quebec; Geological Survey of Canada, Open File 8753; 1 .zip file; https://doi:10.4095/327572

Desbarats, A.J., Percival, J.B., Pelchat, P., Sekerka, J., Bilot, I., Girard, I., and Gammon, P., 2020b. Geoenvironmental characterization of ferroniobium slag, Saint Lawrence Columbium Mine, Oka, Quebec; Geological Survey of Canada, Open File 8752; 1 .zip file; https://doi:10.4095/327565

Desbarats, A.J., Percival, J.B., Bilot, I., Polivchuk, M.J., and Venance, K.E., 2022. Drainage chemistry of mine tailings from a carbonatite-hosted Nb-REE deposit, Oka, Quebec, Canada; Applied Geochemistry, 138, 105216. https://doi.org/10.1016/j.apgeochem.2022.105216

Desbarats, A.J., Balkwill-Tweedie, H., Percival, J.B., Al, T., 2024. Geoenvironmental characteristics of ferroniobium slag from the Saint Lawrence Columbium mine, Oka, Quebec, Canada. Submitted to Applied Geochemistry.

Dold, B, 2020. Sourcing of critical elements and industrial minerals from mine waste – The final evolutionary step back to sustainability of humankind? Jour. Geochemical Exploration, 219, 106638; https://doi.org/10.1016/j.gexplo.2020.106638

Eby, G.N., 1975. Abundance and distribution of the rare-earth elements and yttrium in the rocks and minerals of the Oka carbonatite complex, Quebec. Geochim. Cosmochim. Acta., 39, 597-620.

ECCC, 2018. Canadian Climate Normals, Environmental and Climate Change Canada; website accessed in May 2018. http://climate.weather.gc.ca/climate_normals

Ecozones, 2018. The Ecological Framework of Canada; Website accessed in 2018. http://ecozones.ca

Gibson, C. E., Kelebek, S., and Aghamirian, M., 2015. Niobium oxide mineral flotation: A review of relevant literature and the current state of industrial operations; International Journal of Mineral Processing, 137, 82-97; https://doi.org/10.1016/j.minpro.2015.02.005

Gold, D. P., Vallée, M., and Charette, J.P., 1967. Economic geology and geophysics of the Oka Alkaline Complex, Quebec; Canadian Institute of Mining and Metallurgy Bulletin, 60, 1131-1144.

Gold, D. P., and Vallée, M., 1969. Field Guide to the Oka Area: Description and Itinerary; Government of Quebec, Department of Natural Resources, Mines Branch, Rep. S-101, 37p.

Hornig-Kjarsgaard, I., 1998. Rare earth elements in sövitic carbonatites and their mineral phases; Journal of Petrology, 39, 11-12, 2105-2121.

Lentz, D., Eby, N., Lavoie, S. and Park, A., 2006. Diatremes, dykes, and diapirs: Revisiting the ultra-alkaline to carbonatitic magmatism of the Monteregian Hills; Guide book, Field Trip B4, GAC/MAC Joint Annual Meeting, Montréal, Quebec, 48p.

Lottermoser, B.G., 2011. Recycling, re-use and rehabilitation of mine wastes; Elements, 7, 405-410; https://doi: 10.2113/gselements.7.6.405

McDonough, W. F., and Sun, S., 1995. The composition of the Earth; Chemical Geology, 120, 223-253.

MDDELCC, 2016. Guide d'intervention - Protection des sols et réhabilitation des terrains contaminés. Ministère du Développement durable, de l'Environnement et de la Lutte contre les changements climatiques. 210 p.

Mitchell, R. H., 2015. Primary and secondary niobium mineral deposits associated with carbonatites; Ore Geology Reviews, 64, 626-641; https://doi.org/10.1016/j.oregeorev.2014.03.010.

Modreski, P. J., T.J. Armbrustmacher, and D.B. Hoover, 1995. Carbonatite deposits; In chapter 6 of Preliminary Compilation of Descriptive Geoenvironmental Mineral Deposit Models, (ed.) E.A. du Bray, U.S. Geological Survey, Open-File Report 95-831, p. 47-49.

Mudd, G.M., Jowitt, S.M., Werner, T.T., 2017. The world's by-product and critical metal resources part 1: Uncertainties, current reporting practices, implications, and grounds for optimism; Ore Geology Reviews, 86, 924-938; http://dx.doi.org/10.1016/j.oregeorev.2016.05.001

Mulenshi, J., Gilbricht, S., Chelgani, S.C., Rosenkranz, J., 2021. Systematic characterization of historical tailings for possible remediation and recovery of critical metals and minerals – The Yxsjöberg case; Jour. Geochemical Exploration, 226, 106777; https://doi.org/10.1016/j.gexplo.2021.106777

Nikonow, W., Rammlmair, D., and Furche, M., 2019. A multidisciplinary approach considering geochemical reorganization and internal structure of tailings impoundments for metal exploration. Applied Geochemistry, 104, 51–59; https://doi.org/10.1016/j.apgeochem.2019.03.014

Niocan, 2010. Modèle géologique et estimation des ressources de niobium de la zone S-60, Oka, Quebec; NI 43-101 Technical Report, prepared by S. Lavoie and J.-C. Caron for Niocan Inc., 182 p.

NRCan, 2022. Mining value from waste: Sampling plan development and tailings sampling protocol. Report prepared by Pinchin for Natural Resources Canada, Critical Minerals and Industry Support Division, September 30, 2022, 30pp.

Petruk, W. and Owens, D.R., 1975. Electron microprobe analyses for pyrochlores from Oka, Quebec; Canadian Mineralogist, 13, 282-285.

Richardson, D. G., and Birkett, T.C., 1996. Carbonatite-associated deposits; In: Geology of Canadian Mineral Deposit Types, (eds.) O.R. Eckstrand, W.D. Sinclair, and R.I. Thorpe, Geology of Canada Series, No. 8, 541-558, Geological Survey of Canada, Ottawa, Ontario.

Seal, R.R. II, Piatak, N.M., 2017. Environmental attributes and resource potential of mill tailings from diverse mineral deposit types; In Wolkersdorfer, C., Sartz, L., Sillanpää, M., Häkkinen, A. (Eds.) Proceedings of the International Mine Water Association Conference, Mine Water and the Circular Economy, Lappeenranta, Finland, 25–30 June 2017; 603-609.

Simandl, G. J., Paradis, S., 2018. Carbonatites: related ore deposits, resources, footprint, and exploration methods; Applied Earth Science (Trans. Austral. Inst. Min. Metall.); https://doi.org/10.1080/25726838.2018.1516935

SLC, 1962. St. Lawrence Columbium and Metals Corporation, Annual Report, 8 p.

SLC, 1963. St. Lawrence Columbium and Metals Corporation, Annual Report, 8 p.

SLC, 1964. St. Lawrence Columbium and Metals Corporation, Annual Report, 16 p.

SLC, 1966. St. Lawrence Columbium and Metals Corporation, Annual Report, 28 p.

SLC, 1967. St. Lawrence Columbium and Metals Corporation, Annual Report, 16 p.

SLC, 1968. St. Lawrence Columbium and Metals Corporation, Annual Report, 18 p.

SLC, 1969. St. Lawrence Columbium and Metals Corporation, Annual Report, 24 p.

SLC, 1970. St. Lawrence Columbium and Metals Corporation, Annual Report, 24 p.

SLC, 1971. St. Lawrence Columbium and Metals Corporation, Annual Report, 20 p.

SLC, 1972. St. Lawrence Columbium and Metals Corporation, Annual Report, 28 p.

Spears, B.M., Brownlie, W.J., Cordell, D., Hermann, L., Mogollón, J.M., 2022. Concerns about global phosphorous demand for lithium-iron-phosphate batteries in the light electric vehicle sector; Nature Communications Materials, 3:14; https://doi.org/10.1038/s43246-022-00236-4

Steger, H.F., and Bowman, W.S., 1981. Niobium Ore Oka-1 – A Certified Reference Material; Canada Centre for Mineral and Energy Technology (CANMET) report 81-1E, Energy, Mines and Resources Canada, Ottawa, 16 p.

Strong, W.L., Zoltai, S.C., and Ironside, G.R., 1989. Ecoclimatic regions of Canada; Ecological Land Classification Series 23, Can. Wildlife Service, Environment Canada, Ottawa, 122 p.

Suppes, R., and Heuss-Aßbichler, S., 2021. Resource potential of mine wastes: A conventional and sustainable perspective on a case study tailings mining project. Journal of Cleaner Production, 297, 126446; https://doi.org/10.1016/j.jclepro.2021.126446

Treiman, A.H., and Essene, E.J., 1985. The Oka carbonatite complex, Quebec: geology and evidence for silicate-carbonate liquid immiscibility. Amer. Mineral., 70, 1101-1113.

Vitti, C., Arnold, B.J., 2022. The reprocessing and revalorisation of critical minerals in mine tailings; Mining, Metallurgy and Exploration, 39, 49-54; https://doi.org/10.1007/s42461-021-00524-6

Weng, Z. H., Jowitt, S.M., Mudd, G.M., and Haque, N., 2013. Assessing rare earth element mineral deposit types and links to environmental impacts; Applied Earth Science (Trans. Austral. Inst. Min. Metall.), 122, 2, 83-96. http://doi:10.1179/1743275813Y.0000000036.

Werner, T.T., Mudd, G.M., Jowitt, S.M., 2017; The world's by-product and critical metal resources part II: A method for quantifying the resources of rarely reported metals; Ore Geology Reviews, 80, 658-675; http://dx.doi.org/10.1016/j.oregeorev.2016.08.008

Woolley, A. R., Kjarsgaard, B.A., 2008. Carbonatite occurrences of the world: map and database. Geol. Surv. Canada, Open File 5796, 28p.

WSP, 2018. Caractérisation environnementale, Site minier St-Lawrence Columbium, Oka (Quebec); report prepared for le Ministère de l'Énergie et des Ressources Naturelles by WSP Canada Inc., March 2018, 61p. and appendices. https://mern.gouv.qc.ca › demande-acces › document_19-04-003-C

Zurevinski, S. E., and Mitchell, R.H., 2004. Extreme compositional variation of pyrochlore-group minerals at the Oka carbonatite complex, Quebec: Evidence of magma mixing? Canadian Mineralogist, 42, 1159-1168.